Two RNA-binding proteins mediate the sorting of miR223 from mitochondria into exosomes

Liang Ma[1], Jasleen Singh[1], and Randy Schekman[1 *]

[1]Department of Molecular and Cell Biology, Howard Hughes Medical Institute, University of California, Berkeley, United States.

[*]For correspondence: schekman@berkeley.edu

Abstract

Fusion of multivesicular bodies (MVBs) with the plasma membrane results in the secretion of intraluminal vesicles (ILVs), or exosomes. The sorting of one exosomal cargo RNA, miR223, is facilitated by the RNA-binding protein, YBX1 (Shurtleff et al., 2016). We found that miR223 specifically binds a “cold shock" domain (CSD) of YBX1 through a 5’ proximal sequence motif UCAGU that may represent a binding site or structural feature required for sorting. Prior to sorting into exosomes, most of the cytoplasmic miR223 resides in mitochondria. An RNA-binding protein localized to the mitochondrial matrix, YBAP1, appears to serve as a negative regulator of miR223 enrichment into exosomes. miR223 levels decreased in the mitochondria and increased in exosomes after loss of YBAP1. We observed YBX1 shuttle between mitochondria and endosomes in live cells. YBX1 also partitions into P body granules in the cytoplasm (Liu et al., 2021). We propose a model in which miR223 and likely other miRNAs are stored in mitochondria and are then mobilized by YBX1 to cytoplasmic phase condensate granules for capture into invaginations in the endosome that give rise to exosomes.

Introduction

Extracellular vesicles (EVs) bud from the plasma membrane or are secreted when multivesicular bodies (MVB) fuse with the plasma membrane to release a population of vesicles called exosomes. EVs and their cargos are highly dependent on their membrane source. Microvesicles released by budding from the plasma membrane are a heterogeneous

population of EVs ranging in size from 30 nm to 1000 nm (Cocucci et al., 2009). Exosomes are 30 nm to 150 nm in size and originate as vesicles invaginated into the interior of an MVB to form intraluminal vesicles (ILVs) (Harding et al., 1983).

Many RNAs are selectively sorted into EVs, especially small RNAs. Several studies have indicated that RNA binding proteins (RNPs) may be involved in the enrichment of RNAs into EVs (Mukherjee et al., 2016; Santangelo et al., 2016; Teng et al., 2017; Villarroya-Beltri et al., 2013). However, many of these studies used sedimentation at ~100,000 g to collect EVs, which may also collect RNP particles not enclosed within membranes which complicates the interpretation of these data. To address this question, we previously developed buoyant density-based methods to separate EVs from non-vesicular aggregates and found that EVs form two distinct populations of high and low buoyant density (Shurtleff *et al.*, 2016; Temoche-Diaz et al., 2020) . We found that some miRNAs are selectively enriched in a high buoyant density vesicle fraction characterized by an enrichment in the exosomal marker protein CD63, whereas the low buoyant density EVs are fairly non-selective in the capture of miRNAs (Temoche-Diaz et al., 2019). We developed a cell-free reaction to identify YBX1 as required for miR223 sorting into exosomes and demonstrated that it plays an important role in the enrichment of miR223 into exosomes in HEK293T cells (Shurtleff *et al.*, 2016). We subsequently found that phase separated YBX1 condensates selectively recruit miR223 *in vitro* and sort it into exosomes in cells (Liu *et al.*, 2021). In this study we report that YBX1 directly and specifically binds miR223 by its “cold shock” domain (CSD). We have identified a sequence motif, UCAGU, that facilitates the sorting of

miR223 into exosomes. We also found a significant fraction of cytoplasmic miR223 localized within mitochondria, tightly associated with the mitochondrial envelope and that a mitochondrial RNA-binding protein, YBAP1, may control the transfer of miR223 from mitochondria to exosomes.

Results

YBX1 directly and specifically binds miR223

We previously documented that YBX1 facilitates miR223 sorting into exosomes (Shurtleff *et al.*, 2016) and that exosomal miR223 is decreased in YBX1 knockout cells (Liu *et al.*, 2021). We reexamined the enrichment and confirmed that exosomal miR223 was decreased in exosomes purified from YBX1 KO cells (Figure 1a). We used a Nanosight particle tracking device to quantify buoyant density purified vesicles and found that knockout of YBX1 did not affect exosome secretion (Figure 1 supplement 1).

Whereas the importance of YBX1 for miR223 sorting has been established, the mechanism of their interaction was not known. To examine the direct interaction of YBX1 and miR223, we used an electrophoretic mobility shift assay (EMSA) with purified recombinant YBX1, expressed in insect cells (Figure 1 supplement 2a), and chemically synthetic miR223 and miR190, a cytoplasmic miRNA that is not enriched in exosomes. Purified YBX1 was titrated and incubated with 5' fluorescently labeled miR223 at 30℃ for 30min. miR223-YBX1 complexes were separated by electrophoresis and detected by in-gel fluorescence. The EMSA data showed that YBX1 directly and specifically bound to miR223, but ~140-fold less well with miR190 (Figure 1b-c). The measured Kd for YBX1:miR223 was 4.2nM (Figure 1d).

98 YBX1 has three major domains including an N-terminal alanine/proline-rich
99 (A/P) domain, a central cold shock domain (CSD) and a C-terminal domain
100 (CTD) (Figure 1e). To explore which specific domain of YBX1 binds
101 miR223, we constructed a series of fragments: the A/P domain, CSD and
102 CTD. The YBX1 fragments were expressed in and purified from insect cells
103 (Figure 1 supplement 2b). EMSA data showed that the A/P domain and
104 CTD had little or no affinity for miR223, whereas the CSD domain bound
105 miR223 but with an affinity much reduced compared to full length YBX1
106 (Figure 1f). We then constructed two combined fragments of the A/P and
107 CSD and CSD and CTD domains (Figure 1 supplement 2c). The EMSA
108 data showed that the A/P domain was dispensable whereas binding of
109 miR223 to CSD plus CTD was comparable to full length YBX1 (Figure 1g).

110 YBX1-F85A in the CSD domain was reported to block the YBX1-specific
111 binding of mRNA (Lyons et al., 2016). Purified YBX1-F85A protein failed to
112 bind miR223 (Figure 1g, Figure 1 supplement 2c). These data suggest that
113 YBX1 directly and specifically binds miR223 via the CSD. The CTD of
114 YBX1 did not appear to bind miR223 but may somehow facilitate a higher
115 affinity interaction of the CSD with miR223.

116 A binding or structural motif on miR223 that promotes interaction 117 with YBX1 and enrichment into exosomes

118 We next sought to determine the miR223 sequence motif responsible for
119 interaction with YBX1 and enrichment into exosomes. We used an EMSA
120 competition assay with a series of miR223 mutants. Purified YBX1 and 5'
121 fluorescently labeled miR223 were incubated with miR223 mutant
122 constructs titrated in a range from 1nM to 1μM. miR223 variants in a
123 binding domain should not compete for interaction of YBX1 with 5'

124 fluorescently tagged miR223 whereas variations in sequences irrelevant to
125 interaction would compete. Using this EMSA competition assay to screen
126 the miR223 binding motif, we found that the competitive binding of
127 miR223mut (3-6) and miR223mut (4-7) were decreased (Figure 2
128 supplement 1). This suggested that the sequence UCAGU was critical for
129 interaction with YBX1. To test this directly, we employed a variant
130 sequence, termed miR223mut, where the UCAGU was substituted with
131 AGACA. As a positive control, we employed a variant of miR190,
132 miR190sort, where the sequence AUAUG was substituted with UCAGU
133 (Figure 2a). EMSA data showed a ~27-fold reduced YBX1 interaction of
134 with miR223mut whereas the affinity of miR190sort with YBX1 was
135 increased ~8 fold compared to wt sequences.

136 To test whether this motif is critical for miR223 enrichment into exosomes,
137 we purified exosomes from 293T cells transiently transfected to
138 overexpress one of the four miRNA constructs (Figure 2d). RT-qPCR data
139 showed that the level of miR223 in exosomes was ~ 4-fold dependent on
140 the putative exosomal sorting motif (Figure 3e) and the enrichment of
141 miR190sort into exosomes was increased ~5-fold compared to miR190 WT
142 (Figure 2f).

143 In previous work, we developed a cell-free reaction to test the biochemical
144 requirement for YBX1 in the sorting of miR223 into vesicles formed with
145 membranes and cytosol isolated from broken HEK293 cells (Shurtleff et al.
146 2016). In this work we showed that the sorting of miR223 and of a CD63-
147 luciferase fusion protein into an enclosed membrane were coincidentally
148 inhibited by GW4869 an inhibitor of neutral sphingomyelinase (NS2) known
149 to interfere with exosome biogenesis and secretion. On this basis, we

150 concluded that the cell-free reaction recapitulated the sorting event leading
151 to the packaging of miR223 into exosomes.

152 We refined this assay to measure the incorporation of ^{32}P-5' end-labeled wt
153 and mutant miR223 into vesicles formed *in vitro*. Isolated membranes and
154 cytosol were incubated with ^{32}P-labled wt or mutant miR223 at 30 °C for
155 20min, after which RNase I was added to digest any unpackaged miRNA.
156 Controls including 1% Triton X-100 were used to measure background
157 RNase resistant radiolabel. Samples were resolved on a gel for visual and
158 quantitative evaluation of membrane sequestered RNA (Figure 2g and 2h).
159 The results suggested that the UCAGU motif is critical for miR223
160 packaging into vesicles in the cell-free reaction.

161 Taken together the results in Fig. 2 show that the miR223 sequence
162 UCAGA promotes the binding of YBX1 in order to sort the miRNA into
163 vesicles formed in cells and in a cell-free reaction. We suggest this sorting
164 facilitates the export of miR223 in exosomes secreted from HEK293 cells.

165 **Mitochondria contribute to miR223 enrichment into exosomes.**

166 In a recent study we showed that YBX1 is sorted into P-bodies in cells and
167 that these biomolecular condensates may initiate the sorting of miR223 into
168 vesicles budding into the interior of endosomes (Liu *et al.*, 2021; Shurtleff *et*
169 *al.*, 2016). Mitochondria represent another apparent intracellular location of
170 miR223 (Wang et al., 2020). We used cell fractionation of homogenates of
171 HEK293 cells to evaluate the subcellular distribution of endogenous
172 miR223. Fractionation was evaluated by immunoblot using marker proteins
173 characteristic of various cell organelles (Figure 3a). Analysis of RNA
174 extracted from isolated membranous organelles confirmed that miR223 but

175 not miR190 was significantly enriched in mitochondria but not in ER or
176 cytosol (Figure 3b, Figure 3 supplement 1a) (Wang *et al.*, 2020).

177 To determine the localization of miR223 on or within mitochondria, we
178 prepared mitoplasts using digitonin to strip away the mitochondrial outer
179 membrane followed by fractionation on a Percoll density gradient.
180 Immunoblots of the enriched mitochondria and isolated mitoplasts showed
181 that the outer membrane, marked by Tom20, was largely removed with
182 retention of the inner membrane marker Tim23 (Figure 3c). RNA was
183 extracted from the purified mitoplast and RT-qPCR data indicated that
184 miR223 was enriched along with mRNA for COX1, but not with nuclear U6
185 snRNA (Figure 3d).

186 As an independent means to assess the localization of cytoplasmic miR223,
187 we used immunoprecipitation to purify mitochondria. Isolated mitochondria
188 were then converted to mitoplasts by osmotic shock and treated with
189 proteinase K and RNase. Immunoblots of the immunoprecipitated
190 mitochondria and isolated mitoplasts showed that the outer membrane,
191 marked by Tom20, and intermembrane space, marked by AIF, were largely
192 removed with retention of the mitochondrial matrix marker citrate synthase
193 (Figure 3e). RNA was extracted from the immunoprecipitated mitochondria
194 and mitoplasts and RT-qPCR data indicated that miR223 was enriched
195 along with mRNA for COX1, but not with miR190 or nuclear U6 snRNA
196 (Figure 3f).

197 We also used immunoprecipitated mitochondria (Figure 3 supplement 1b)
198 and either Triton X-100 to solubilize the membrane or freeze-thaw to allow
199 the matrix and envelope fractions to be separated by centrifugation.
200 Mitochondrial membrane proteins, such as Tom20 and COX IV, were

201 solubilized and retained in the supernatant fraction (Figure 3 supplement
202 1c). The freeze-thaw regimen released citrate synthase to a supernatant
203 fraction whereas Tom20 and COX IV sedimented in the pellet fraction. RNA
204 was extracted from the detergent supernatant and pellet fractions where we
205 found similar distributions of COX1 and miR223, neither of which were as
206 readily solubilized as the inner and outer membrane proteins (Figure 3
207 supplement 1d). RT-qPCR quantification of fractions from the freeze-thaw
208 regimen showed that both COX1 mRNA and miR223 remained largely
209 associated with the sedimentable membrane fraction (Figure 3 supplement
210 1e). We conclude that miR223 is enclosed within mitochondria, possibly in
211 association with the inner membrane.

212 We sought a test of the role of mitochondria in the secretion of miR223 in
213 exosomes. For this purpose, we generated cells depleted of mitochondria
214 (Correia-Melo et al., 2017). U-2 OS cells expressing GFP-parkin were
215 treated with CCCP for 48h, conditions that cause mitochondria to be
216 removed by mitophagy. We confirmed mitochondrial depletion after CCCP
217 treatment by RT-qPCR of mitochondrial COX1 mRNA (Figure 3g) and
218 immunoblot of the mitochondrial inner membrane marker Tim23 (Figure 3h).
219 We then compared the levels of both miR223 and miR190 from GFP-parkin
220 expressing U-2 OS cells with and without CCCP treatment. RT-qPCR data
221 showed that miR223, but not miR190, increased 3-fold in cells treated with
222 CCCP (Figure 3j). To test the possibility that miR223 accumulated in cells
223 as a result of a failure of mobilization into exosomes, we compared the
224 miR223 levels in exosomes purified from untreated and CCCP treated cells
225 (Fig. 3 j). Although exosome secretion, as measured with a CD63-
226 luciferase marker, did not change after CCCP treatment (Figure 3

227 supplement 2a), we found that CCCP treatment lowered the amount of
228 miR223 in EVs 4-fold (Figure 3j). The increase in cellular at the expense of
229 exosomal miR223 may reflect a critical role for mitochondria in the
230 mobilization of this RNA to exosomes.

231 **YBAP1 binds miR223 in the mitochondria and in vitro.**

232 In the course of purifying a tagged version of YBX1 from 293T cells, we
233 observed another protein that copurified and found that it corresponded to
234 YBAP1 (Figure 4a, b). Such a complex of YBX1 and YBAP1 has previously
235 been reported (Matsumoto et al., 2005). We confirmed that purified YBX1
236 and YBAP1 bind each other by coexpression and affinity purification from
237 insect cells (Figure 4 supplement 1b). YBAP1 is a mitochondrial matrix
238 protein with a standard N-terminal transit peptide sequence (Muta et al.,
239 1997). We confirmed this mitochondrial localization in U-2 OS cells
240 expressing Tom22-mCherry transiently transfected with a YBAP1-GFP
241 construct (Figure 4c-d). We also showed that YBAP1 is localized within
242 mitochondria by performing a proteinase K protection assay on purified
243 mitochondria. Mitochondria were isolated from non-transfected cells and
244 exposed to proteinase K in the presence or absence of Triton X-100 and
245 the degradation of YBAP1 was evaluated by immunoblot. YBAP1 was
246 resistant to proteinase K digestion as was the mitochondrial inner
247 membrane marker Tim23. Both were degraded by proteinase treatment in
248 the presence of Triton X-100 (Figure 4e), consistent with the localization of
249 YBAP1 within mitochondria.

250 To test whether YBAP1 was bound to miR223 in mitochondria, we used
251 YBAP1 immunoprecipitation with mitochondria purified by fractionation on a
252 Percoll density gradient (Figure 4f). RT qPCR data showed that

253 mitochondrial miR223 was immunoprecipitated by YBAP1 antibody but not
254 by a control antibody (Figure 4g). To determine whether the YBAP1 and
255 miR223 interaction was direct, we used the EMSA assay and found that
256 purified YBAP1 bound miR223, but not miR190. The YBAP1 interaction
257 with miR223 was not dependent on the RNA sequence motif responsible
258 for YBX1 binding (Figure 4 supplement 2a-b). Taken together, these data
259 suggest that YBAP1 binds miR223 in mitochondria and *in vitro*.

260 **YBAP1 may control the transit of miR223 from mitochondria to**
261 **exosomes**

262 To investigate the function of YBAP1 in the transit of miR223 into
263 exosomes, we generated a 293T YBAP1 KO cell line and compared the
264 level of miR223 enrichment in exosomes and mitochondria isolated from
265 WT and mutant cells (Figure 5a, b). Although knockout of YBAP1 did not
266 change exosome secretion (Figure 5 supplement 1a), RT-qPCR analysis
267 showed that miR223 decreased 2-fold in mitochondria but increased 8-fold
268 in exosomes purified from mutant and WT cells, respectively (Figure 5c).
269 This apparent inverse relationship is consistent with a role for YBAP1
270 protein in the retention of miR223 in mitochondria.

271 **YBX1 puncta shuttled from mitochondria to endosomes**

272 In previous work we reported the localization of YBX1 to P-bodies and
273 suggested this may represent an intermediate stage in the concentrative
274 sorting of miRNAs for secretion in exosomes (Liu *et al.*, 2021). In other
275 earlier work, P-bodies were seen in association with mitochondria (Huang
276 et al., 2011). To explore this possibility, we visualized endogenous YBX1
277 and YBAP1 by IF and observed YBX1 puncta colocalized with mitochondria

(Figure 6a, b). In order to detect the proximity of endosomes to this point of contact between YBX1 puncta and mitochondria, we used U-2 OS cells transfected with Rab5(Q79L)-mCherry, which we employed previously to enlarge and detect the internalization of YBX1 into endosomes (Liu *et al.*, 2021). We then used three color visualization of the U-2 OS cells also transfected with YFP-YBX1 and mito-BFP. Time-lapse imaging showed YBX1 puncta in close proximity to mitochondria or endosomes, followed quickly by transfer between them (Figure 6c, d). Taken together, these data suggest a mechanism whereby miR223 stored in mitochondria, possibly sequestered by YBAP1, may be captured in a tighter interaction with YBX1 in P-bodies and delivered to endosomes for sorting and secretion in exosomes.

Discussion

Selected miRNAs are sorted, some with very high fidelity, into invaginations in the endosome that give rise to exosomes secreted from cultured human cells and likely from many if not all cells in metazoan organisms. The means by which these miRNAs are sorted and the possible extracellular functions they serve is a subject of interest in normal and disease physiology. Here we report the role of the RNA-binding protein YBX1 and a sorting or structural signal on one target RNA, miR223, and the indirect path miR223 may take from storage in mitochondria into exosomes.

We have identified a sequence motif on miR223, UCAGU, responsible for high affinity interaction with YBX and for sorting into vesicles formed in a cell-free reaction as well as for secretion in exosomes by HEK293 cells.

303 Previously we performed this in vitro packaging assay in the presence of an
304 inhibitor (GW4869) of neutral sphingomyelinase (NS2). This inhibitor has
305 been shown to reduce the secretion of exosomes and exosome-associated
306 miRNAs in other studies (Li et al., 2013; Trajkovic et al., 2008; Yuyama et
307 al., 2012). In our cell-free assay, GW4869 inhibited the protection of CD63-
308 luciferase and miR-223 at concentrations known to inhibit the activity of
309 NS2 in partially purified enzyme fractions (Shurtleff *et al.*, 2016). We
310 concluded that our cell-free reaction provides a model that mimics aspects
311 of exosome biogenesis.

312 The YBX1 protein has three distinct domains, one of which, the cold-shock
313 domain (CSD) appears to be the principal site for RNA binding, including at
314 least one critical residue, F85, required for binding miR223 as well as other
315 RNAs (Lyons *et al.*, 2016). The C-terminal domain (CTD) includes an
316 intrinsically disordered domain (IDR) that promotes the formation of a
317 liquid-liquid phase separation likely responsible for the organization of
318 YBX1 in P-bodies (Liu *et al.*, 2021). This domain does not itself interact with
319 RNA, but it appears to facilitate the folding or stabilization of the CSD to
320 promote high affinity binding to miR223.

321 In other work using a similar approach, we identified two separate sorting
322 signals, a 5'UGGA and a 3'UUU, on miR122 to which the RNA-binding
323 protein La binds *en route* to secretion in exosomes by the breast cancer
324 cell line MDA-MB-231(Temoche-Diaz *et al.*, 2019). Other distinct sorting
325 signals and their cognate RNA-binding proteins have been documented in
326 different cell lines. miRNAs with a GGAG sorting motif recognized by a
327 sumolyated form of hnRNPA2B1 was shown to be enriched in exosomes
328 (Villarroya-Beltri *et al.*, 2013). Another sequence, AAUGC, was found to be

329 enriched in exosomal miRNA and dependent on the RNA-binding protein
330 FMR1 for miRNA secretion (Wozniak et al., 2020). Diverse cell lines and
331 likely tissues appear to invoke distinct sorting signals decoded by different
332 RNA-binding proteins. Many of the proteins may engage in biomolecular
333 condensates such as P-bodies as a mechanism to sort RNAs for secretion
334 (Liu *et al.*, 2021).

335 miR223 appears to be an example of a number of small nuclear-encoded
336 RNAs localized to mitochondria (Jeandard et al., 2019). In some cases
337 these RNAs, such as tRNAs, serve an essential function such as in
338 mitochondrial protein synthesis, however, for miRNAs with no obvious
339 mitochondrial genome target, the function remains unclear (Jeandard *et al.*,
340 2019). Nonetheless, others have documented the localization of these
341 miRNAs enclosed within the mitochondrion and in the case of miR223, it
342 appears to be tightly associated with the inner membrane. The exact
343 organization and function of miR223 in this location remains to be
344 investigated but in the context of exosomal secretion, the mitochondrial
345 localization appears to serve as a reservoir.

346 In relation to the mitochondrial localization of miR223, we found a
347 mitochondrial RNA-binding protein, YBAP1, that copurified with a tagged
348 form of YBX1 expressed in HEK293 cells. YBAP1 has previously been
349 reported to interact with YBX1 and independently found associated with
350 mitochondria where its localization is dependent on an N-terminal transit
351 peptide sequence (Muta *et al.*, 1997). The association of mitochondrial
352 YBAP1 and cytoplasmic YBX1 was reproduced by coexpression of
353 recombinant forms of the two proteins in baculovirus-infected SF9 cells
354 (Figure 4 supplement 1b). YBAP1 binds miR223 selectively but with an

355 affinity significantly below that of YBX1 (Figure 4h-j). Although YBX1 does
356 not localize to the mitochondrion, the stable interaction of the complex may
357 suggest a transient relationship, perhaps during the biogenesis of YBAP1
358 as it transits from the cytoplasm into the mitochondrion.

359 A functional relationship between YBAP1 and YBX1 is suggested by the
360 reduction in miR223 in mitochondria and increase in secretion of miR223 in
361 exosomes secreted from YBAP1 KO cells (Fig. 5). In contrast, removal of
362 mitochondria by treatment of cells with CCCP resulted in an increase in
363 cytoplasmic miR223 at the expense of secretion in exosomes (Fig. 3).
364 Although YBAP1 may facilitate the retention of miR223 within mitochondria,
365 mitochondrial RNA import and export may serve an independent role in the
366 selective capture of miRNAs by YBX1 in cytoplasmic P-body condensates.
367 YBX1 puncta appear to shuttle between mitochondria and endosomes at
368 which point miR223 bound to YBX1 may be further sorted into
369 invaginations budding into the interior of endosomes.

370 The highly selective nature of miRNA sorting and secretion in exosomes
371 suggests an important role in the trafficking of miRNAs between cells.
372 Numerous studies have suggested a role for secreted miRNAs in recipient
373 cells (Cha et al., 2015; Mittelbrunn et al., 2011; Pegtel et al., 2010; Valadi
374 et al., 2007). Nonetheless, as miRNAs ordinarily act stoichiometrically on
375 target mRNAs, the extremely low abundance and copy number of
376 miRNAs/vesicle is hard to reconcile with such a functional role of secreted
377 miRNA (Chevillet et al., 2014; Shurtleff et al., 2017) . Our observation that
378 the bulk of cellular miR223 is held within mitochondria suggests an
379 alternative role in some structural or regulatory process, perhaps essential

380 for mitochondrial homeostasis, controlled by the selective extraction of
381 unwanted miRNA into RNA granules and further by secretion in exosomes.

382

383 **Materials and methods**

384 Key resources table

Reagent type (species) or resource	Designation	Source or reference	Identifiers	Additional information
Cell line (Spodoptera frugiperda)	Sf9	Other		Cell culture facility at UC Berkeley
Cell line (Homo sapiens)	HEK 293T cells	Other		Cell culture facility at UC Berkeley
Cell line (Homo sapiens)	HEK 293T-YBX1 KO cells	Other		Obtained by CRISPR-Cas9 in Schekman Lab
Cell line (Homo sapiens)	HEK 293T-YBAP1 KO	This study		Obtained by CRISPR-Cas9 in Schekman Lab
Cell line (Homo sapiens)	HEK 293T-3xHA-EGFP-OMP25	This study		Obtained by overexpression of pLJM1-3XHA-EGFP-OMP25 in Schekman lab
Cell line (Homo sapiens)	U-2OS cells	Other		Cell culture facility at UC Berkeley
Cell line (Homo sapiens)	U-2OS Parkin-GFP cells	This study		Obtained by overexpression of Parkin-GFP in Schekman lab
Recombinant DNA reagent	pFastBac His6 MBP N10 TEV LIC	Addgene	RRID: Addgene_30116	N/A

	cloning vector (4C)			
Recombinant DNA reagent	Tom22-mCherry (plasmid)	This study		Gift of Dr Li Yu lab
Recombinant DNA reagent	His-MBP-YBX1 (plasmid)	This study		To express YBX1 in insect cells. Plasmid maintained in Schekman lab
Recombinant DNA reagent	His-MBP-YBX1(1-51) (plasmid)	This study		To express YBX1(1-51) in insect cells. Plasmid maintained in Schekman lab
Recombinant DNA reagent	His-MBP-YBX1(52-129) (plasmid)	This study		To express YBX1(52-129) in insect cells. Plasmid maintained in Schekman lab
Recombinant DNA reagent	His-MBP-YBX1(130-324) (plasmid)	This study		To express YBX1(1-51) in insect cells. Plasmid maintained in Schekman lab
Recombinant DNA reagent	His-MBP-YBX1(1-129) (plasmid)	This study		To express YBX1(1-129) in insect cells. Plasmid maintained in Schekman lab
Recombinant DNA reagent	His-MBP-YBX1(F85A) (plasmid)	This study		To express YBX1(F85A) in insect cells. Plasmid maintained in Schekman lab
Recombinant DNA reagent	His-MBP-YBAP1 (plasmid)	This study		To express YBAP1 in insect cells. Plasmid maintained in Schekman lab
Recombinant DNA reagent	Mito-BFP	This study		Gift of Dr. Samantha Lewis lab
Recombinant DNA reagent	mCherry-Rab5(Q79L)	Addgene	RRID: Addgene_35138	

	(plasmid)			
Recombinant DNA reagent	pLJM1-3XHA-EGFP-OMP25	This study		To express 3xHA-EGFP-OMP25 in HEK293T cells. Plasmid maintained in Schekman lab
Antibody	Anti-YBX1 (Rabbit polyclonal)	Abcam	RRID: AB_1950384	WB 1:1000
Antibody	Anti-YBAP1 (Mouse monoclonal)	Santa Cruz	RRID: AB_10611471	WB 1:1000
Antibody	Anti-YBAP1(Rabbit polyclonal)	Thermo Fisher Scientific	RRID: AB_2638956	WB 1:1000
Antibody	Anti-Tim23 (Mouse monoclonal)	BD Biosciences	RRID: AB_398754	WB 1:1000
Antibody	Anti-Tom20 (Mouse monoclonal)	Abcam	RRID: AB_945896	WB 1:1000
Antibody	Anti-Calnexin (Rabbit polyclonal)	Abcam	RRID: AB_2069006	WB 1:2000
Antibody	Anti-HA (Rabbit monoclonal)	Cell Signaling	RRID: AB_1549585	WB 1:1000
Antibody	Anti-COX IV (Rabbit Monoclonal)	Cell signaling	RRID: AB_2085424	WB 1:1000
Antibody	Anti-Citrate Synthase (Rabbit monoclonal)	Cell signaling	RRID: AB_2665545	WB 1:1000
Antibody	Anti-Rab5 (Rabbit monoclonal)	Cell signaling	RRID: AB_2300649	WB 1:1000
Antibody	Anti-LAMP1 (Rabbit monoclonal)	Cell signaling	RRID: AB_2687579	WB 1:1000
Antibody	Anti-GRP78 (Rabbit polyclonal)	Abcam	RRID: AB_2119834	WB 1:3000
Antibody	Anti-GADPH	Cell signaling	RRID: AB_561053	WB 1:5000

	(Rabbit monoclonal)			
Antibody	Anti-alpha Tubulin (Mouse monoclonal)	Abcam	RRID: AB_2241126	WB 1:5000
Antibody	Anti-beta Actin (Mouse monoclonal)	Abcam	RRID: AB_449644	WB 1:5000
Software, algorithm	Image Studio Lite	LICOR		https://www.licor.com/bio/image-studio-lite/
Software, algorithm	FIJI	NIH	RRID: SCR_002285	https://fiji.sc/
Software, algorithm	Prism 9	GraphPad	RRID: SCR_002798	https://www.graphpad.com

Cell lines and cell culture

All immortalized cell lines were obtained from the UC-Berkeley Cell Culture Facility and were confirmed by short tandem repeat (STR) profiling and tested negative for mycoplasma contamination. HEK 293T cells were cultured in DMEM with 10% FBS(VWR), NEAA (Gibco, Cat No: 11140050) and 1mM Sodium Pyruvate (Gibco, Cat No: 11360070). For exosome production, we seeded cells at 10~20% confluency in 150 mm tissue culture dishes (Fisher Scientific, Cat No: 12-565-100) containing 30ml of exosome-free medium. Exosomes were collected from 80% confluent cells (~48h).

Exosome purification

Conditioned medium was harvested from 80-90% confluent HEK 293T cultured cells. All procedures were performed at 4 ℃. Cells and large debris

399 were removed by centrifugation in a Sorvall R6+ centrifuge at 1,000xg for
400 15 min followed by 10,000xg for 15 min using a FIBERlite F14-6x500y rotor.
401 The supernatant fraction was then centrifuged onto a 60% sucrose cushion
402 in a buffer with 10mM HEPES (pH 7.4) and 0.85% w/v NaCl at ~100,000 x
403 g (28,000 RPM) for 1.5h in a SW32Ti rotor. The interface over the sucrose
404 cushion was collected and pooled for an additional centrifugation onto a
405 2ml 60% sucrose cushion at ~120,000 x g (31,500 RPM) for 15h using an
406 SW41Ti rotor. The first collected interface was measured by refractometry
407 and adjusted a sucrose concentration not exceeding 21%. For bulk
408 purification, the EVs collected from the interface over the sucrose cushion
409 after the first SW41Ti centrifugation were mixed with 60% sucrose to a final
410 volume of 10ml (the concentration of sucrose ~50%). One ml of 40% and
411 1ml of 10% sucrose were sequentially overlaid and the samples were
412 centrifuged at ~150,000 x g (36,500 rpm) for 15h in an SW41Ti rotor. The
413 exosomes were located at the 10%/40% interface and collected for RNA
414 extraction or immunoblot.

415 **Density gradient isolation of mitochondria and mitoplasts**

416 Mitochondria were isolated according to a well-established published
417 protocol (Wang *et al.*, 2020). HEK293T Cells were harvested at 80%
418 confluency and were homogenized in 6 vol of HB buffer (225 mM mannitol,
419 25 mM sucrose, 0.5% BSA, 0.5 mM EGTA, 30 mM Tris–HCl, pH 7.4, and
420 protease inhibitors) in a prechilled Dounce homogenizer (Kontes). The
421 lysate was centrifuged and the postnuclear supernatant was collected.
422 Crude mitochondria were centrifuged at 6,300 x g for 8 min, washed once
423 with MRB buffer (250 mM mannitol, 0.5 mM EGTA, and 5 mM HEPES, pH
424 7.4), resuspended in 1ml MRB buffer, laid over a 30% Percoll solution (9ml)

425 and centrifuged at 95,000g for 45min. The buoyant, purified fraction of
426 mitochondria was collected for further analysis. For mitoplast purification,
427 crude mitochondria were resuspended into 10 vol MRB buffer with 0.2
428 mg/ml digitonin and incubated on ice for 15 min. Digitonin-treated crude
429 mitochondria were laid over a 30% Percoll solution (9ml) and centrifuged at
430 95,000g for 45 min. A buoyant, purified fraction of mitoplasts was collected
431 for further analysis.

432 **YBAP1 immunoprecipitation from mitochondria**

433 After the Percoll gradient purification, the enriched mitochondria were
434 diluted 2x into MRB buffer and centrifuged at 12,000g for 10 min. The
435 mitochondrial pellet was lysed in 0.5ml RIPA buffer (50mM Tris-HCl, pH 7.5,
436 150mM NaCl, 2mM EDTA, 1% DDM, 1mM PMSF) containing protease
437 inhibitors (1mM 4-aminobenzamidine dihydrochloride, 1 μg/ml antipain
438 dihydrochloride, 1 μg/ml aprotinin, 1 μg/ml leupeptin, 1 μg/ml chymostatin,
439 1 mM phenylmethylsulphonyl fluoride, 50 μM N-tosyl-L-phenylalanine
440 chloromethyl ketone and 1 μg/ml pepstatin) and RNase inhibitors, followed
441 by centrifugation at 12,000g for 10 min. Supernatant fractions were
442 incubated with 10ul washed protein A Dynabeads (ThermoFisher Scientific,
443 Catalog number: 10001D) and 0.5ug mouse monoclonal IgG antibody and
444 rotated at 4 ℃ for 1h. A magnetic rack was used to remove protein A beads
445 and the resulting supernatant fractions were incubated with 40ul washed
446 protein A Dynabeads and 4ug YBAP1 antibody or mouse IgG antibody and
447 rotated at 4 ℃ overnight. The beads were collected using a magnetic rack,
448 washed 3x with 1ml of RIPA buffer, and collected for immunoblot and RNA
449 extraction.

450 **Mitochondria immunoprecipitation**

451 Mito-IP was performed as previously described with slight modifications
452 (Chen et al., 2016). The mito-IP cell-line was grown to ~90% confluency in
453 15cm dishes. All the subsequent steps of mito-IP were performed using
454 ice-cold buffers either in a cold-room or on ice. Cells ($2x10^7$) were washed
455 twice with 10ml of PBS and then harvested in 10ml of mito-IP buffer (10mM
456 KH2PO4, 137mM KCl) containing protease inhibitors (1mM 4-
457 aminobenzamidine dihydrochloride, 1 µg/ml antipain dihydrochloride, 1
458 µg/ml aprotinin, 1 µg/ml leupeptin, 1 µg/ml chymostatin, 1 mM
459 phenylmethylsulphonyl fluoride, 50 µM N-tosyl-L-phenylalanine
460 chloromethyl ketone and 1 µg/ml pepstatin) and TCEP 0.5mM. The final
461 mito IP buffer also contained 6ml of OptiPrep™ (Sigma®) per 100ml. Cells
462 were collected at 700xg for 5 min and resuspended in 1ml of mito-IP buffer
463 per 15cm plate and then lysed using 5-10 passes through a 22G needle. A
464 post-nuclear supernatant (PNS) fraction was obtained after centrifuging the
465 lysate at 1500xg for 10 min to remove unbroken cells and nuclei. Whenever
466 necessary, a fraction of PNS was saved for immunoblot analysis. The
467 resulting PNS was incubated with 100 µl of anti-HA magnetic beads
468 (Sigma®) pre-equilibrated in the mito-IP buffer in 1.5ml microcentrifuge
469 tubes and then gently rotated on a mixer for 15min. The beads were
470 collected using a magnetic rack and washed 3x for 5min with 1ml of mito-IP
471 buffer.

472 For mitoplast purification by osmotic shock, the supernatant was discarded
473 after the final wash of the mito-IP sample, and the beads were gently
474 resuspended in 200 µl of hypotonic osmotic shock buffer (OSB) containing
475 20 mM HEPES at pH 7.4. The resuspended sample was incubated on ice

476 for 30 min and then the beads were centrifuged at 15,000 g for 15 min to
477 sediment mitochondria/mitoplasts. Beads were then resuspended in 100 µl
478 of KPBS and proteinase K was added to achieve a final concentration of 10
479 µg/ml and samples were incubated on a rotating mixer at 4^0 C for 15 min.
480 Subsequently, PMSF was added to a final concentration of 1 mM, along
481 with a protease inhibitor cocktail, and the sample was incubated on ice for
482 5 min. Next, 2.5 units of RNase ONE (Promega) was added to the sample,
483 which was further incubated on a rotating mixer at room temperature for 15
484 min. For protein analysis, the sample was eluted directly in the SDS loading
485 buffer. Alternatively, Trizol was added to the sample to stop the reaction for
486 RNA purification.

487 To assess their quality, we assayed the immunoprecipitated mitochondria
488 for the following protein markers by immunoblotting using the rabbit primary
489 antibodies- anti-HA (1:1000), anti-COX IV (1:1000), anti-TOM20 (1:1000),
490 anti-Citrate Synthase (1:1000), anti-RAB5 (1:1000), anti-LAMP1 (1:2000),
491 anti-GAPDH (1:5000), and anti-GRP78 (Abcam®) (1:3000). All of the above
492 antibodies were sourced from Cell Signaling Technology®, unless stated
493 otherwise. As a negative control, non-transduced HEK293T cells were
494 used in these experiments to assess the non-specific capture of the marker
495 proteins.

496 **Mitochondrial Fractionation**

497 One mito-IP was performed per sample as described above. To ensure an
498 even distribution of mitochondria across the samples, we pooled washed
499 beads from all the IPs and equally distributed aliquots for subsequent
500 treatments. Mitochondria were lysed in a 50µl final volume using either 1%
501 vol/vol Triton X-100 (final concentration) or by three sequential rounds of
502 freeze/thaw using liquid-nitrogen, as indicated. Urea was added to a final

503 concentration of 3M. After a 10 min incubation on ice, samples were
504 centrifuged at 15000xg for 15 min and supernatant and pellet fractions
505 were collected as indicated. The total fractionated mitochondria were
506 analyzed by immunoblotting for various mitochondrial markers. To analyze
507 the specific RNA content of total or fractionated mitochondria, we extracted
508 RNA using Trizol™ (Invitrogen®) as per manufacturer's recommendations
509 followed by q-PCR.

510 **In vitro packaging of miR223 and miR223mut**

511 Preparation of membranes and cytosol

512 The membrane and cytosol fractions were prepared from HEK293T cells as
513 previously described with slight modifications (Shurtleff *et al.*, 2016;
514 Temoche-Diaz *et al.*, 2020). All steps were carried out in either the cold-
515 room or on ice using ice-cold buffers and pre-chilled equipment. Briefly,
516 HEK293T cells (80% confluency) were washed twice with PBS and then
517 harvested in the homogenization buffer (HB) (250 mM sorbitol, 20mM
518 HEPES-KOH pH 7.4) containing protease inhibitor cocktail (1mM 4-
519 aminobenzamidine dihydrochloride, 1 µg/ml antipain dihydrochloride, 1
520 µg/ml aprotinin, 1 µg/ml leupeptin, 1 µg/ml chymostatin, 1 mM
521 phenylmethylsulphonyl fluoride, 50 µM N-tosyl-L-phenylalanine
522 chloromethyl ketone and 1 µg/ml pepstatin). The cell pellet was obtained by
523 centrifuging the cells at 500xg for 5 min. After discarding the supernatant,
524 cells were weighed and resuspended in two volumes of HB followed by
525 lysis with 5-10 passages through a 22G needle. The lysate was centrifuged
526 at 1500xg for 10 min to remove unbroken cells and nuclei to obtain a PNS
527 which was then centrifuged at 20,000xg for 30 min to obtain a membrane
528 fraction. The supernatant from above was centrifuged at 150,000xg for 30
529 min using a TLA-55 rotor (Beckman Coulter ®) and the resulting
530 supernatant was used as the cytosol fraction (~6mg protein/ml).
531 Membranes from the first 20,000xg sedimentation were resuspended in 1
532 ml of HB and centrifuged again at 20,000xg for 30 min. The pellet fraction
533 was resuspended in one volume of HB and rested on an ice block for a
534 minimum of 10 min until the insoluble components and debris settled at the
535 bottom of the tube. The finely resuspended material in the resulting
536 supernatant fraction was then transferred to a new microcentrifuge tube (to
537 avoid the settled debris) and was used as the membrane fraction.

538 Preparation of radiolabeled miR223 and miR223mut substrates

539 HPLC purified miR223 and miR223mut oligos were obtained from IDT®. A
540 stock solution of these oligos (1µl of a 10µM) was 5'-end-labeled using
541 T4PNK (NEB®) and 5µl of ATP, [γ-32P]- 6000Ci/mmol 10mCi/ml EasyTide
542 (PerkinElmer® BLU502Z250UC) as per manufacturer's recommendations
543 in a 50µl reaction volume. T4PNK was heat-inactivated at 70°C for 15 min.
544 Unincorporated radionucleotides were removed by passing through
545 PerformaTM spin columns (EdgeBio®). The flow-through (radiolabeled
546 substrate) was collected and stored at -20°C until further use.

547 *In vitro* miR223 packaging reaction

548 Wherever indicated, 10µl of cytosol (~5 mg/ml), 17µl of membranes, 2µl of
549 radiolabeled substrate, 9µl of 5x incorporation buffer (400 mM KCl, 100 mM
550 $CaCl_2$, 60 mM HEPES-NaOH, pH 7.4, 6 mM, MgOAc), 4.5µl of 10x ATP
551 regeneration system (400 mM creatine phosphate, 2 mg/ml creatine
552 phosphokinase, 10 mM ATP, 20 mM HEPES pH 7.2, 250 mM sorbitol, 150
553 mM KOAc, 5 mM MgOAc), 1µl of ATP (100mM, Promega®), 0.5µl of GTP
554 (100mM, Promega®), 1µl of Ribolock™ (40U/µl, Invitrogen®) were mixed to
555 setup a 45µl *in vitro* packaging reaction. In samples without the cytosol or
556 membranes, the final reaction volumes were adjusted to 45µl using HB.
557 The reactions were incubated at either 30°C or on ice, as indicated, for 15
558 min. Following the incubation, the indicated samples were subjected to
559 RNAse ONE™ (Promega®) using 10U of the enzyme in the presence of
560 urea (300mM final concentration) in a total reaction volume of 60µl.
561 Wherever indicated, TritonX-100 was added to a final concentration of 1%.
562 The RNAse treatments were carried out for 20 min at 30°C followed by
563 RNA extraction using DirectZol™ (Zymo Research®) kits as per
564 manufacturer's protocol. RNA was precipitated overnight at -20°C by the
565 addition of 3 vol of ethanol, 1/10th volume of 3M sodium acetate (pH5.2)
566 and 30µg Glycoblue™ reagent (Invitrogen®). Precipitated RNA was
567 sedimented at 16,000xg for 30 min followed by washing with ice-cold 70%
568 ethanol. The RNA pellet was resuspended in 2X RNA loading dye (NEB®)
569 and heated for 5 min at 70°C. RNA was separated using a 15% denaturing
570 polyacrylamide gel, followed by gel drying using a vacuum gel dryer (Model
571 583, Biorad®). Radioactive bands were visualized by phosphorimaging

572 using a Kodak® storage phosphor screen and the Pharos FX™ Plus
573 Molecular Imager (Biorad®).

574 **Immunoblots**

575 Cell lysates and other samples were prepared by adding 2% SDS and
576 heated at 95 ℃ for 10min. Protein was quantified using a BCA Protein
577 Assay Kit (Thermo Fisher Scientific) and appropriate amounts were mixed
578 with 5x SDS loading buffer. Samples were heated at 95℃ for 10min and
579 separated on 4–20% acrylamide Tris-glycine gradient gels (Life
580 Technologies). Proteins were transferred to PVDF membranes (EMD
581 Millipore, Darmstadt, Germany) and the membrane was blocked with 5%
582 fat-free milk powder in TBST and incubated for 1 h at room temperature or
583 overnight at 4°C with primary antibodies. Blots were then washed in 3
584 washes of TBST for 10 min each. Membranes were incubated with anti-
585 rabbit or anti-mouse secondary antibodies (GE Healthcare Life Sciences,
586 Pittsburgh, PA) for 1h at room temperature and rinsed in 3 washes of TBST
587 for 10 min each. Blots were developed with ECL-2 reagent (Thermo Fisher
588 Scientific). Primary antibodies used in this study were as follows: anti-
589 Tim23 (BD, 611222), Calnexin (Abcam, ab22595), Actin (Abcam, ab8224),
590 Tubulin (Abcam, ab7291), YBAP1 (Santa Cruz Biotechnology, sc-271200).

591 **Immunofluorescence**

592 Cells were cultured on 12mm round coverslips (corning) and were fixed
593 with 4% EM-grade paraformaldehyde (Electron Microscopy Science,
594 Hatfield, PA) in PBS pH7.4 for 10 min at room temperature. Cells were then
595 washed 3x with PBS for 10min each, treated with permeabilizing buffer (10%
596 FBS in PBS) containing 0.1% saponin for 20min and treated in blocking

597 buffer for 30min. Subsequently, cells were incubated with primary
598 antibodies in permeabilizing buffer for 1h at room temperature, washed 3x
599 with PBS for 10 min each and incubated with secondary antibodies in
600 permeabilizing buffer for 1h at room temperature and finally washed 3x with
601 PBS for 10 min each. Cells were mounted on slides with Prolong Gold with
602 DAPI (Thermo Fisher Scientific, P36931). Primary antibodies used in the
603 immunofluorescence studies were as follows: anti-YBX1 (Abcam, ab12148),
604 YBAP1 (Santa Cruz Biotechnology, sc-271200). Images were acquired with
605 Zeiss LSM900 confocal microscope and analyzed with the Fiji software
606 (http://fiji.sc/Fiji).

607 **Quantitative real-time PCR**

608 Cellular and EV RNAs were extracted using a mirVana miRNA isolation kit
609 (Thermo Fisher Scientific, AM1560) or Direct-zol RNA Miniprep kits (Zymo
610 Research). Taqman miRNA assays for miRNA detection were purchased
611 from Life Technologies. Assay numbers were: hsa-miR-223-3p, 002295;
612 hsa-mir-190–5 p, 000489; U6 snRNA, 001973. Total RNAs were quantified
613 using RNA bioanalyzer (Agilent). Taqman qPCR master mix with no
614 Amperase UNG was obtained from Life Technologies for reverse
615 transcription. For mRNA, RevertAid First Strand cDNA Synthesis Kit
616 (Thermo Scientific, K1621) was used for reverse transcription. COX1 qPCR
617 primers: Forward-5'-TCTCAGGCTACACCCTAGACCA-3', Reverse-5'-
618 ATCGGGGTAGTCCGAGTAACGT-3'. GAPDH qPCR primers: Forward-5'-
619 CTGACTTCAACAGCGACACC-3', Reverse-5'-
620 TAGCCAAATTCGTTGTCATACC-3'. Quantitative real-time PCR was
621 performed using an QuantStudio™ 5 Real-Time PCR System (Applied
622 Biosystems™)

623 **Protein Purification**

624 Twin Strep tag hybrid YBX1 was expressed and the protein was isolated
625 48h after PEI-mediated transfection of 293T cells. Cells were resuspended
626 in PBS and collected by centrifugation for 5 min at 600g. Pellet fractions
627 were resuspended in 35 ml lysis buffer (50mM Tris-HCl (pH 8),150mM
628 NaCl,1mM EDTA, 2mM DTT, 1mM PMSF and 1 x protease inhibitor
629 cocktail). After sonication of the cell suspension the crude lysate was
630 centrifuged for 60 min at 20,000 rpm at 4 °C. The resulting supernatant
631 fraction was incubated with 2 ml Strep-Tactin® Sepharose® resin (IBA, 2-
632 1201-010) for 1 h. Strep-Tactin® Sepharose® resin samples were
633 transferred to columns (18ml) and protein-bound beads were washed with
634 60ml wash buffer (50mM Tris-HCl (pH 8), 500mM NaCl, 1mM EDTA, 2mM
635 DTT) until no protein was eluted as monitored by the Bio-Rad protein assay
636 (Bio-Rad, Catalog #5000006). Proteins were eluted with 10 ml elution
637 buffer (50mM Tris-HCl (PH=8),150mM NaCl, 10mM desthiobiotin, 1mM
638 EDTA, 2mM DTT) and concentrated using an Amicon Ultra Centrifugal
639 Filter Unit (50 kDa, 4 ml) (Fisher Scientific, EMD Millipore). Proteins were
640 further purified by gel filtration chromatography (Superdex-200, GE
641 Healthcare) with columns equilibrated in storage buffer (50 mM Tris-HCl
642 7.4, 500 mM KCl, 5 % glycerol, 1 mM DTT). Peak fractions corresponding
643 to the appropriate fusion protein were pooled, concentrated, and distributed
644 in 10 µl aliquots in PCR tubes, flash-frozen in liquid nitrogen and stored at -
645 80 °C. Protein concentration was determined by known concentrations of
646 BSA assessed by Coomassie Blue staining.

647 Tagged (6xHis) and maltose-binding protein hybrid genes were expressed
648 in baculovirus-infected SF9 insect cells (Lemaitre et al., 2019). Insect cell

649 cultures (1 l, $1x10^6$ cells/ml) were harvested 48 h after viral infection and
650 collected by centrifugation for 20 min at 2000 rpm. The pellet fractions were
651 resuspended in 35 ml lysis buffer (50 mM Tris-HCl 7.4, 0.5 M KCl, 5 %
652 glycerol, 10mM imidazole, 0.5 µl/ml Benzonase nuclease (Sigma, 70746–3),
653 1 mM DTT, 1 mM PMSF and 1 x protease inhibitor cocktail). Cells were
654 lysed by sonication and the crude lysate was centrifuged for 60 min at 20,
655 000 rpm at 4 °C. After centrifugation, the supernatant fraction was
656 incubated with 2 ml Ni-NTA His-Pur resin (Thermo Fisher, PI88222) for 1 h.
657 Ni-NTA resin samples were transferred to columns (18ml) and protein-
658 bound beads were washed with 60ml lysis buffer until no protein was eluted
659 as monitored by the Bio-Rad protein assay (Bio-Rad, Catalog #5000006).
660 Proteins were eluted with 10 ml elution buffer (50 mM Tris-HCl 7.4, 0.5 M
661 KCl, 5 % glycerol, 500mM imidazole). The eluted sample was incubated
662 with 2 ml amylose resin (New England Biolabs, E8021L) for 1 h at 4°C.
663 Amylose resin samples were transferred to columns and protein-bound
664 beads were washed with 60ml lysis buffer until no protein was eluted as
665 monitored by the Bio-Rad protein assay. Proteins were eluted with 10 ml
666 elution buffer (50 mM Tris-HCl 7.4, 500 mM KCl, 5 % glycerol, 50 mM
667 maltose) and were concentrated using an Amicon Ultra Centrifugal Filter
668 Unit (50 kDa, 4 ml) (Fisher Scientific, EMD Millipore). Proteins were further
669 purified by gel filtration chromatography (Superdex-200, GE Healthcare)
670 with columns equilibrated in storage buffer (50 mM Tris-HCl 7.4, 500 mM
671 KCl, 5 % glycerol, 1 mM DTT). Peak fractions corresponding to the
672 appropriate fusion protein were pooled, concentrated, and distributed in 10
673 µl aliquots in PCR tubes, flash-frozen in liquid nitrogen and stored at –
674 80 °C. Protein concentration was determined by known concentrations of
675 BSA based on Coomassie blue staining.

676 **CRISPR/Cas9 genome editing**

677 A pX330-based plasmid expressing Venus fluorescent protein (Shurtleff *et*
678 *al.*, 2016) was used to clone the gRNAs targeting YBAP1. A CRISPR guide
679 RNA targeting the first exon of the YBAP1 open reading frame was
680 designed following the CRISPR design website
681 (http://crispor.tefor.net/crispor.py): CGCTGCGTGCCCCGTGTGCT.
682 Oligonucleotides encoding gRNAs were annealed and cloned into pX330-
683 Venus as described (Cong et al., 2013). HEK293T cells were transfected
684 by Lipofectamine 2000 for 48h at low passage number, trypsinized and
685 sorted for single, Venus positive cells in 96 well plates by a BD Influx cell
686 sorter. YBAP1 knockout candidates were confirmed by immunoblot. HEK
687 293T YBX1 knockout cells were generously provided by Dr. Xiaoman Liu
688 (Liu *et al.*, 2021).

689 **Electrophoretic mobility shift assay**

690 Fluorescently labeled RNAs (5'-IRD800CWN) for detecting free and
691 protein-bound RNA were ordered from Integrated DNA Technologies (IDT,
692 Coralville, IA). EMSA was performed as described with some modification
693 (Rio, 2014). Briefly, 1 nM of IRD800CWN-labeled RNA was incubated with
694 increasing amounts of purified proteins, ranging from 500 pM - 1 μM.
695 Buffer E was used in this incubation (25 mM Tris pH8.0, 100 mM KCl, 1.5
696 mM MgCl2, 0.2 mM EGTA, 0.05% Nonidet P-40, 1 mM DTT, 5% glycerol,
697 50 ug/ml heparin). Reactions were incubated at 30 ℃ for 30min then chilled
698 on ice for 10 min. Samples were mixed with 6x loading buffer (60 mM KCl,
699 10 mM Tris pH 7,6, 50% glycerol, 0.03% (w/v) xylene cyanol). Mixtures
700 (5ul) were loaded onto a 6% native polyacrylamide gel and electrophoresed

701 at 200V for 45mins in a cold room. The fluorescence signal was detected
702 using an Odyssey CLx Imaging System (LI-COR Biosciences, Lincoln, NE).
703 The software of the Odyssey CLx Imaging System was used to quantify
704 fluorescence. To calculate Kds, we fitted used Hill equations with quantified
705 data points.

706 **CD63-Nluc exosome secretion assay**

707 The CD63-Nluc exosome secretion assay was carried out as described
708 (Williams et al., 2023). Briefly, cells stably expressing CD63-Nluc were
709 cultured in 24-well plates until reaching approximately 80% confluence. All
710 subsequent procedures were performed at 4°C. Conditioned medium (200
711 µl) was collected from the appropriate wells and transferred to
712 microcentrifuge tubes. The tubes were subjected to centrifugation at 1000
713 × g for 15 min to remove intact cells, followed by an additional
714 centrifugation at 10,000 × g for 15 min to eliminate cellular debris.
715 Supernatant fractions (50 µl) were used for measuring CD63-Nluc exosome
716 luminescence. Cells were kept on ice and washed once with cold PBS,
717 and then lysed in 200 µl of PBS containing 1% TX-100 and protease
718 inhibitor cocktail.

719 For the measurement of CD63-Nluc exosome secretion, a master mix was
720 prepared by diluting the Extracellular NanoLuc Inhibitor at a 1:1000 ratio
721 and the NanoBRET Nano-Glo Substrate at a 1:333 ratio in PBS (Promega,
722 Madison, WI, USA). Aliquots of the Nluc substrate/inhibitor master mix (100
723 µl) were added to 50 µl of the supernatant fraction obtained from the
724 medium-speed centrifugation. The mixture was briefly vortexed, and
725 luminescence was measured using a Promega GlowMax 20/20

726 Luminometer (Promega, Madison, WI, USA). Following luminescence
727 measurements, 1.5 µl of 10% TX-100 was added to each reaction tube to
728 achieve a final concentration of 0.1% TX-100. Samples were vortexed
729 briefly, and luminescence was measured again. For intracellular
730 normalization, the luminescence of 50 µl of cell lysate was measured using
731 the Nano-Glo Luciferase Assay kit (Promega, Madison, WI, USA) following
732 the manufacturer's instructions. The exosome production index (EPI) for
733 each sample was calculated using the formula: EPI = ([medium] - [medium
734 + 0.1% TX-100])/cell lysate.

735

736 **Data availability**

737 All data generated or analyzed in this study are included in the manuscript
738 and supporting files. Source data files have been provided for Figure 1b,
739 Figure 1c, Figure 1f, Figure 1g, Figure 1-figure supplement 2a-c, Figure 2b,
740 Figure 2g, Figure 2-figure supplement 1a-f, Figure 3a, Figure 3c, Figure 3e,
741 Figure 3h, Figure 3 supplement 1b-c, Figure 4a, Figure 4b, Figure 4e,
742 Figure 4f, Figure 4h, Figure 4i, Figure 4-figure supplement 1a-b, Figure 4-
743 figure supplement 2a, Figure 5b.

744

745 **Funding**

746 **Howard Hughes Medical Institute (Investigator)**

747 **Randy Schekman**

748 The funders had no role in study design, data collection and interpretation,
749 or the decision to submit the work for publication.

750

751 ## Acknowledgements

752 We thank Dr. Samantha Lewis for advice about localization to mitochondria
753 and for sharing a plasmid; thanks Matthew J Shurtleff, David Melville,
754 Shenjie Wu, Jordan Ngo, Congyan Zhang, Justin Williams, Morayma M
755 Temoche-Diaz for suggestions and reading and editing the manuscript. We
756 also thank staff at the UC Berkeley shared facilities, the Cell Culture Facility,
757 the Flow Cytometry Facility and QB3-Berkeley (The California Institute for
758 Quantitative Biosciences at UC Berkeley). LM and JS are supported as
759 Research Associates of the HHMI. RS is an Investigator of the HHMI, a
760 Senior fellow of the UC Berkeley Miller Institute of Science and Scientific
761 Director of Aligning Science Across Parkinson's Disease.

762

763 ## References

764 Cha, D.J., Franklin, J.L., Dou, Y., Liu, Q., Higginbotham, J.N., Demory Beckler,
765 M., Weaver, A.M., Vickers, K., Prasad, N., Levy, S., et al. (2015). KRAS-
766 dependent sorting of miRNA to exosomes. Elife *4*, e07197. 10.7554/eLife.07197.
767 Chen, W.W., Freinkman, E., Wang, T., Birsoy, K., and Sabatini, D.M. (2016).
768 Absolute Quantification of Matrix Metabolites Reveals the Dynamics of
769 Mitochondrial Metabolism. Cell *166*, 1324-1337 e1311.
770 10.1016/j.cell.2016.07.040.
771 Chevillet, J.R., Kang, Q., Ruf, I.K., Briggs, H.A., Vojtech, L.N., Hughes, S.M.,
772 Cheng, H.H., Arroyo, J.D., Meredith, E.K., Gallichotte, E.N., et al. (2014).
773 Quantitative and stoichiometric analysis of the microRNA content of exosomes.
774 Proc Natl Acad Sci U S A *111*, 14888-14893. 10.1073/pnas.1408301111.
775 Cocucci, E., Racchetti, G., and Meldolesi, J. (2009). Shedding microvesicles:
776 artefacts no more. Trends Cell Biol *19*, 43-51. 10.1016/j.tcb.2008.11.003.

Cong, L., Ran, F.A., Cox, D., Lin, S., Barretto, R., Habib, N., Hsu, P.D., Wu, X., Jiang, W., Marraffini, L.A., and Zhang, F. (2013). Multiplex genome engineering using CRISPR/Cas systems. Science *339*, 819-823. 10.1126/science.1231143.

Correia-Melo, C., Ichim, G., Tait, S.W., and Passos, J.F. (2017). Depletion of mitochondria in mammalian cells through enforced mitophagy. Nat Protoc *12*, 183-194. 10.1038/nprot.2016.159.

Harding, C., Heuser, J., and Stahl, P. (1983). Receptor-mediated endocytosis of transferrin and recycling of the transferrin receptor in rat reticulocytes. J Cell Biol *97*, 329-339. 10.1083/jcb.97.2.329.

Huang, L., Mollet, S., Souquere, S., Le Roy, F., Ernoult-Lange, M., Pierron, G., Dautry, F., and Weil, D. (2011). Mitochondria associate with P-bodies and modulate microRNA-mediated RNA interference. J Biol Chem *286*, 24219-24230. 10.1074/jbc.M111.240259.

Jeandard, D., Smirnova, A., Tarassov, I., Barrey, E., Smirnov, A., and Entelis, N. (2019). Import of Non-Coding RNAs into Human Mitochondria: A Critical Review and Emerging Approaches. Cells *8*. 10.3390/cells8030286.

Li, J., Liu, K., Liu, Y., Xu, Y., Zhang, F., Yang, H., Liu, J., Pan, T., Chen, J., Wu, M., et al. (2013). Exosomes mediate the cell-to-cell transmission of IFN-alpha-induced antiviral activity. Nat Immunol *14*, 793-803. 10.1038/ni.2647.

Liu, X.M., Ma, L., and Schekman, R. (2021). Selective sorting of microRNAs into exosomes by phase-separated YBX1 condensates. Elife *10*. 10.7554/eLife.71982.

Lyons, S.M., Achorn, C., Kedersha, N.L., Anderson, P.J., and Ivanov, P. (2016). YB-1 regulates tiRNA-induced Stress Granule formation but not translational repression. Nucleic Acids Res *44*, 6949-6960. 10.1093/nar/gkw418.

Matsumoto, K., Tanaka, K.J., and Tsujimoto, M. (2005). An acidic protein, YBAP1, mediates the release of YB-1 from mRNA and relieves the translational repression activity of YB-1. Mol Cell Biol *25*, 1779-1792. 10.1128/MCB.25.5.1779-1792.2005.

Mittelbrunn, M., Gutierrez-Vazquez, C., Villarroya-Beltri, C., Gonzalez, S., Sanchez-Cabo, F., Gonzalez, M.A., Bernad, A., and Sanchez-Madrid, F. (2011). Unidirectional transfer of microRNA-loaded exosomes from T cells to antigen-presenting cells. Nat Commun *2*, 282. 10.1038/ncomms1285.

Mukherjee, K., Ghoshal, B., Ghosh, S., Chakrabarty, Y., Shwetha, S., Das, S., and Bhattacharyya, S.N. (2016). Reversible HuR-microRNA binding controls extracellular export of miR-122 and augments stress response. EMBO Rep *17*, 1184-1203. 10.15252/embr.201541930.

Muta, T., Kang, D., Kitajima, S., Fujiwara, T., and Hamasaki, N. (1997). p32 protein, a splicing factor 2-associated protein, is localized in mitochondrial matrix and is functionally important in maintaining oxidative phosphorylation. J Biol Chem *272*, 24363-24370. 10.1074/jbc.272.39.24363.

817 Pegtel, D.M., Cosmopoulos, K., Thorley-Lawson, D.A., van Eijndhoven, M.A.,
818 Hopmans, E.S., Lindenberg, J.L., de Gruijl, T.D., Wurdinger, T., and Middeldorp,
819 J.M. (2010). Functional delivery of viral miRNAs via exosomes. Proc Natl Acad
820 Sci U S A *107*, 6328-6333. 10.1073/pnas.0914843107.
821 Rio, D.C. (2014). Electrophoretic mobility shift assays for RNA-protein complexes.
822 Cold Spring Harb Protoc *2014*, 435-440. 10.1101/pdb.prot080721.
823 Santangelo, L., Giurato, G., Cicchini, C., Montaldo, C., Mancone, C., Tarallo, R.,
824 Battistelli, C., Alonzi, T., Weisz, A., and Tripodi, M. (2016). The RNA-Binding
825 Protein SYNCRIP Is a Component of the Hepatocyte Exosomal Machinery
826 Controlling MicroRNA Sorting. Cell Rep *17*, 799-808.
827 10.1016/j.celrep.2016.09.031.
828 Shurtleff, M.J., Temoche-Diaz, M.M., Karfilis, K.V., Ri, S., and Schekman, R.
829 (2016). Y-box protein 1 is required to sort microRNAs into exosomes in cells and
830 in a cell-free reaction. Elife *5*. 10.7554/eLife.19276.
831 Shurtleff, M.J., Yao, J., Qin, Y., Nottingham, R.M., Temoche-Diaz, M.M.,
832 Schekman, R., and Lambowitz, A.M. (2017). Broad role for YBX1 in defining the
833 small noncoding RNA composition of exosomes. Proc Natl Acad Sci U S A *114*,
834 E8987-E8995. 10.1073/pnas.1712108114.
835 Temoche-Diaz, M.M., Shurtleff, M.J., Nottingham, R.M., Yao, J., Fadadu, R.P.,
836 Lambowitz, A.M., and Schekman, R. (2019). Distinct mechanisms of microRNA
837 sorting into cancer cell-derived extracellular vesicle subtypes. Elife *8*.
838 10.7554/eLife.47544.
839 Temoche-Diaz, M.M., Shurtleff, M.J., and Schekman, R. (2020). Buoyant Density
840 Fractionation of Small Extracellular Vesicle Sub-populations Derived from
841 Mammalian Cells. Bio Protoc *10*, e3706. 10.21769/BioProtoc.3706.
842 Teng, Y., Ren, Y., Hu, X., Mu, J., Samykutty, A., Zhuang, X., Deng, Z., Kumar,
843 A., Zhang, L., Merchant, M.L., et al. (2017). MVP-mediated exosomal sorting of
844 miR-193a promotes colon cancer progression. Nat Commun *8*, 14448.
845 10.1038/ncomms14448.
846 Trajkovic, K., Hsu, C., Chiantia, S., Rajendran, L., Wenzel, D., Wieland, F.,
847 Schwille, P., Brugger, B., and Simons, M. (2008). Ceramide triggers budding of
848 exosome vesicles into multivesicular endosomes. Science *319*, 1244-1247.
849 10.1126/science.1153124.
850 Valadi, H., Ekstrom, K., Bossios, A., Sjostrand, M., Lee, J.J., and Lotvall, J.O.
851 (2007). Exosome-mediated transfer of mRNAs and microRNAs is a novel
852 mechanism of genetic exchange between cells. Nat Cell Biol *9*, 654-659.
853 10.1038/ncb1596.
854 Villarroya-Beltri, C., Gutierrez-Vazquez, C., Sanchez-Cabo, F., Perez-Hernandez,
855 D., Vazquez, J., Martin-Cofreces, N., Martinez-Herrera, D.J., Pascual-Montano, A.,
856 Mittelbrunn, M., and Sanchez-Madrid, F. (2013). Sumoylated hnRNPA2B1

857 controls the sorting of miRNAs into exosomes through binding to specific motifs.
858 Nat Commun *4*, 2980. 10.1038/ncomms3980.
859 Wang, W.X., Prajapati, P., Nelson, P.T., and Springer, J.E. (2020). The
860 Mitochondria-Associated ER Membranes Are Novel Subcellular Locations
861 Enriched for Inflammatory-Responsive MicroRNAs. Mol Neurobiol *57*, 2996-
862 3013. 10.1007/s12035-020-01937-y.
863 Williams, J.K., Ngo, J.M., Lehman, I.M., and Schekman, R. (2023). Annexin A6
864 mediates calcium-dependent exosome secretion during plasma membrane repair.
865 Elife *12*. 10.7554/eLife.86556.
866 Wozniak, A.L., Adams, A., King, K.E., Dunn, W., Christenson, L.K., Hung, W.T.,
867 and Weinman, S.A. (2020). The RNA binding protein FMR1 controls selective
868 exosomal miRNA cargo loading during inflammation. J Cell Biol *219*.
869 10.1083/jcb.201912074.
870 Yuyama, K., Sun, H., Mitsutake, S., and Igarashi, Y. (2012). Sphingolipid-
871 modulated exosome secretion promotes clearance of amyloid-beta by microglia. J
872 Biol Chem *287*, 10977-10989. 10.1074/jbc.M111.324616.

873

874 **Figure legends**

875 **Figure 1.** YBX1 directly and specifically binds miR223.

876 (a.) RT-qPCR analysis of fold change of miR-223 and miR-190 in cells and
877 purified exosomes from 293T WT cells and YBX1 knockout cells. Data are
878 plotted from 3 independent experiments, each independent experiment with
879 triplicate qPCR reactions; error bars represent standard deviations. (b-c.)
880 EMSA assays using 1nM 5' fluorescently labeled miR223 or miR190 and
881 purified YBX1. Purified YBX1 was titrated from 500pM to 1μM. In gel
882 fluorescence was detected. Quantification of (d.) shows the calculated Kd.
883 (e.) Schematic diagrams of the different domains of YBX1. (f.) EMSA assay
884 using 1nM 5' fluorescently labeled miR223 and purified YBX1 truncations.
885 [YBX1(1-51) or YBX1(52-129) or YBX1(130-324).] (g.) EMSA assay using
886 1nM 5' fluorescently labeled miR223 and purified YBX1 truncations
887 [YBX1(1-129) or YBX1(52-324)] or YBX1(F85A) mutant.

888 **Figure 1-figure supplement 1. Knockout of YBX1 did not change**
889 **exosome secretion.**

890 (a.) Exosome numbers are measured by Nanosight NS300. Normalized
891 exosome number from 293T WT and YBX1-KO cells are shown.

892 **Figure 1-figure supplement 2.** Purified YBX1 full length protein and
893 different truncations and mutation.

894 (a-c.) YBX1 full length protein or different truncations were overexpressed
895 and purified from insect cells.

896 **Figure 2.** miR223 sequence motif UCAGU binds YBX1

897 (a.) RNA oligonucleotides corresponding to miR223, miR190 and versions
898 with mutated sorting motif (miR223mut) or mutation to introduce the sorting
899 motif (miR190sort). (b.) EMSA assays using 1nM 5' fluorescently labeled
900 miR223 WT or miR223mut or miR190 WT or miR190sort and purified
901 YBX1. Purified YBX1 was titrated from 500pM to 1μM. In gel fluorescence
902 was detected. (c.) Binding affinity curves as calculated by EMSA data from
903 (b.) (d.) Schematic shows exosome purification with buoyant density
904 flotation in a sucrose step gradient from 293T cells overexpressing miR223
905 WT or mutant or miR190 WT or miR190sort. (e.) RT-qPCR analysis of
906 relative abundance of miR223 or miR223mut detected in exosomes
907 compared to cellular level in 293T cells overexpressing miR223 WT or
908 miR223mut. Data are plotted from 3 independent experiments and error
909 bars represent standard deviations. (f.) RT-qPCR analysis of relative
910 abundance of miR190 or miR190sort detected in exosomes compared to
911 cellular level in 293T cells overexpressing miR190 WT or miR190sort. Data
912 are plotted from 3 independent experiments and error bars represent

913 standard derivations. (g.) *In vitro* packaging assay using ^{32}P 5'end-labeled
914 miR223 and miR223mut. Cell-free packaging of miR223 and miR223mut
915 measured as protected radioactive signal from ^{32}P labeled miR223 and
916 miR223mut. Reactions with or without membrane, cytosol, and 1% Triton
917 X-100, and incubated at 4 or 30 °C are indicated. For the samples
918 containing only cytosol plus membrane at 4 °C, only one-third of the
919 samples were loaded. Each sample was supplemented with 300mM urea
920 to reduce the background signal. (h.) Data quantification showed protected
921 fraction of miR223 and miR223mut as calculated from *in vitro* packaging
922 data shown in (g.)

923 **Figure 2-figure supplement 1.** Screening of exosomal sorting motif of
924 miR223.

925 EMSA competition assay to screen the exosomal sorting motif of miR223.
926 (a.-f.) EMSA competition assay using 1nM 5' fluorescently labeled miR223,
927 32nM purified YBX1 protein and unlabeled miR223 or miR223mutants.
928 Unlabeled miR223 or miR223mutants were titrated from 1nM to 1μM and
929 are given as the ratio of unlabeled miR223/labeled miR223 (wt and mutant).

930 **Figure 3.** Mitochondria contribute to miR223 enrichment into exosomes.

931 (a.) Immunoblot analysis of protein markers for different subcellular
932 fractions isolated from 293T cells. (b.) RT-qPCR analysis of miR223 fold
933 changes of different subcellular fractions isolated from 293T cells relative to
934 cell lysate. (c.) Immunoblot analysis of protein markers for mitoplasts
935 purified from 293T cells by Percoll gradient fractionation (MT: mitochondria;
936 MP: mitoplast). (d.) RT-analysis of COX1 mRNA, miR223 and U6 snRNA
937 fold changes for mitoplasts purified from 293T cells relative to cell lysate.

938 (e.) Immunoblot analysis of protein markers for immunoprecipitated
939 mitochondria and osmotic shock generated mitoplasts. Mitochondria were
940 purified from a 293T 3xHA-EGFP-OMP25 overexpressing cell line using
941 anti-HA magnetic beads. Mitoplasts were purified following mitochondrial
942 immunoprecipitation by osmotic shock, proteinase K and RNase treatment
943 (IP-MT: immunoprecipitated mitochondria; IP-MP: immunoprecipitated
944 mitoplasts). (f.) RT-analysis of COX1 mRNA, miR223, miR190 and U6
945 snRNA fold changes for immunoprecipitaed mitochondria and mitoplasts
946 purified from the 293T 3xHA-EGFP-OMP25 overexpressing cell line. Data
947 are plotted from 3 independent experiments and error bars represent
948 standard deviations. (g.) RT-qPCR analysis of mitochondrial mRNA COX1
949 in U2OS cells expressing GFP-Parkin treated with or without CCCP. Data
950 are plotted from 3 independent experiments and error bars represent
951 standard deviations. (h.) Immunoblot analysis of mitochondrial marker
952 Tim23 in U2OS cells expressing GFP-Parkin treated with or without CCCP.
953 (i.) Schematic of exosome purification from mitochondria depleted GFP-
954 Parkin expressing U2OS cells. (j.) RT-qPCR analysis of fold change of
955 miR-223 and miR-190 in cells and purified exosomes from U2OS cells
956 expressing GFP-Parkin which were treated with or without CCCP. Data are
957 plotted from 3 independent experiments and error bars represent standard
958 deviations.

959 **Figure 3-figure supplement 1.** miR223, but not miR190, enriched in
960 mitochondria.

961 (a.) RT-qPCR analysis of miR190 fold changes in subcellular fractions
962 isolated from 293T cells relative to cell lysate. Data are plotted from 3
963 independent experiments and error bars represent standard deviations. (b.)

964 Mitochondria immunoprecipitation. Mitochondria purified from 293T WT or
965 3xHA-EGFP-OMP25 overexpressing cell line using anti-HA magnetic
966 beads. Immunoblot detection of inner membrane marker COX IV, outer
967 membrane marker TOM20 and mitochondrial matrix protein citrate
968 synthase (CS) but not of the early endosome marker RAB5, lysosome
969 marker LAMP1, cytosol marker GAPDH and ER marker GRP78. (c.)
970 Purified mitochondria from (b.) were treated with 1% Triton X-100 or
971 freeze/thaw using liquid-nitrogen and the supernatant and pellet fractions
972 were collected after centrifugation. Immunoblot analysis of the
973 mitochondrial protein distribution of outer membrane protein TOM20, inner
974 membrane protein COX IV and matrix protein citrate synthase. (d.) and (e.)
975 RT-qPCR analysis of the distribution of COX1 mRNA and miR223 from (c.)
976 Data are plotted from 2 independent experiments and error bars represent
977 standard deviations.

978 **Figure 3-figure supplement 2. Mitochondrial depletion did not change**
979 **exosome secretion.**

980 (a.) CD63-Nluc was stably expressed in the cell lines expressing U2OS-
981 GFP-Parkin. Exosome numbers are measured by luminescence from the
982 conditioned medium of CD63-Nluc cells which were treated with or without
983 CCCP. Normalized exosome production from cells are shown.

984 **Figure 4.** YBAP1 directly and specifically binds miR223.

985 (a.) Strep II-YBX1 was overexpressed in HEK293T cells. Coomassie blue
986 detection of unknown band copurified with YBX1 from 293T cells. (b.)
987 Immunoblot identified unknown band was YBAP1. (c.) Tom22-mCherry
988 expressing U2OS was transfected with a YBAP1-GFP-expressing plasmid,

989 cultured for 12h and observed by confocal microscopy. Scale bar, 10 μm.
990 (d.) Quantification of the fluorescence intensity of the different channels
991 indicated by the solid white line of (c.). (e.) YBAP1 resides in mitochondria.
992 Proteinase K protection assay for YBAP1 using purified mitochondria from
993 293T cells. Samples were treated with or without proteinase K (10 ug/ml)
994 and or Triton X-100 (0.5%). Immunoblots for Tim23, Tom20 and YBAP1
995 are shown. (f.) Mitochondria were purified for immunoprecipitation with
996 YBAP1 antibody. Immunoblot detection of YBAP1 and Tom20. (g.) RT-
997 qPCR analysis of miR223 fold changes of YBAP1 IP samples. Data are
998 plotted from 3 independent experiments and error bars represent standard
999 deviations. (h-i.) EMSA assays using 1nM 5' fluorescently labeled miR223
1000 or miR190. Purified YBAP1 was titrated from 500pM to 1μM. In gel
1001 fluorescence was detected. Quantification of (j.) shown the calculated Kd.

1002 **Figure 4-figure supplement 1.** YBX1 and YBAP1 copurify as a complex
1003 from transfected SF9 cells.

1004 (a.) YBAP1 purified from insect cells which overexpressed His-MBP-
1005 YBAP1. (b.) YBX1 and YBAP1 were copurified from insect cells which
1006 overexpressed His-MBP-YBX1 with untagged YBAP1.

1007 **Figure 4-figure supplement 2.** YBAP1 does not share the same miR223-
1008 binding motif as YBX1.

1009 (a.) EMSA assays using 1nM 5' fluorescently labeled miR223 WT or
1010 miR223mut or miR190 WT or miR190sort and purified YBAP1. Purified
1011 YBAP1 was titrated from 500pM to 1μM. In gel fluorescence was detected.
1012 (b.) Binding affinity curves as calculated by EMSA data from (a.)

1013

1014 **Figure 5.** YBAP1 sequesters miR223 which is released and secreted in
1015 YBAP1 KO cells

1016 (a.) Schematic shows exosome and mitochondria purification from 293T
1017 WT cells and YBAP1 knock out cells for RT-qPCR analysis. (b.) Analysis of
1018 293T WT and CRISPR/Cas9 genome-edited cells by immunoblot for
1019 YBAP1, YBX1 and mitochondrial markers (c.) RT-qPCR analysis of
1020 miR223 enrichment in mitochondria purified from 293T WT cells and
1021 YBAP1 KO cells relative to cell lysate. Data are plotted from 3 independent
1022 experiments and error bars represent standard deviations. (d.) RT-qPCR
1023 analysis of miR223 and miR190 fold change in cells, purified mitochondria
1024 and exosomes from 293T WT cells and YBAP1 KO cells. Data are plotted
1025 from 3 independent experiments and error bars represent standard
1026 deviations.

1027 **Figure 5-figure supplement 1. Knockout of YBAP1 did not change**
1028 **exosome secretion.**

1029 (a.) CD63-Nluc was stably expressed in the 293T WT and YBAP1-KO cell
1030 lines. Exosome production was measured by luminescence of CD63-Nluc
1031 in the conditioned medium of cells which were treated with or without
1032 CCCP. Normalized exosome production from 293T WT and YBAP1-KO
1033 cells are shown.

1034

1035 **Figure 6.** YBX1 puncta relocalize from mitochondria to endosomes.

1036 (a.) YBX1 puncta on the mitochondria. U2OS cells were stained with anti-
1037 YBX1 and anti-YBAP1 antibodies and observed by confocal microscopy.
1038 The right panel shows enlarged regions of interest from the left panel.

1039 Scale bar, 5 μm. (b.) The statistics are of the percentage of YBX1 puncta
1040 detected in proximity to mitochondria. n=30 cells. (c.) YBX1 puncta
1041 relocalize from mitochondria to endosomes. U2OS cells overexpressed
1042 YFP-YBX1, Rab5(Q79L)-mCherry and mito-BFP. Time-lapse images were
1043 acquired with a Zeiss LSM900 confocal microscope. Scale bar, 2 μm. (d.)
1044 The statistics are of YBX1 puncta shuttle events per cell. The data was
1045 represented as violin plots. N=34 cells.

1046 **Figure 7.** Diagram representing a model of miR223 sorting from
1047 mitochondria into exosomes.

1048 Stages in the transfer of miR223 from mitochondria. Cytosolic miR223 is
1049 enriched in mitochondria where it may be sequestered by a weak
1050 interaction with YBAP1. Cytoplasmic YBX1 interacts more tightly with
1051 miR223 which may drive the removal of miR223 from mitochondria. YBX1
1052 in RNA granules may accumulate miR223 removed from mitochondria.
1053 YBX1 puncta may give rise to small particles carrying miR223 for uptake
1054 into endosomes and secretion in exosomes.

1055 **Figure 1 – source data.** Uncropped gel images corresponding to Figure 1.

1056 **Figure 1 – figure supplement 2 – source data.** Uncropped gel images
1057 corresponding to Figure 1 supplement 2.

1058 **Figure 2 – source data.** Uncropped gel images corresponding to Figure 2.

1059 **Figure 2 – figure supplement 1 – source data.** Uncropped gel images
1060 corresponding to Figure 2 supplement 1.

1061 **Figure 3 – source data.** Uncropped immunoblot images corresponding to
1062 Figure 3.

1063 **Figure 3 – figure supplement 1 – source data**. Uncropped immunoblot
1064 images corresponding to Figure 3 supplement 1.

1065 **Figure 4 – source data.** Uncropped immunoblot and gel images
1066 corresponding to Figure 4.

1067 **Figure 4 – figure supplement 1** – source data. Uncropped gel images
1068 corresponding to Figure 4 supplement 1.

1069 **Figure 4 – figure supplement 2** – source data. Uncropped gel images
1070 corresponding to Figure 4 supplement 2.

1071 **Figure 5 – source data**. Uncropped immunoblot images corresponding to
1072 Figure 5.

1073

Figure 1. YBX1 directly and specifically binds miR223

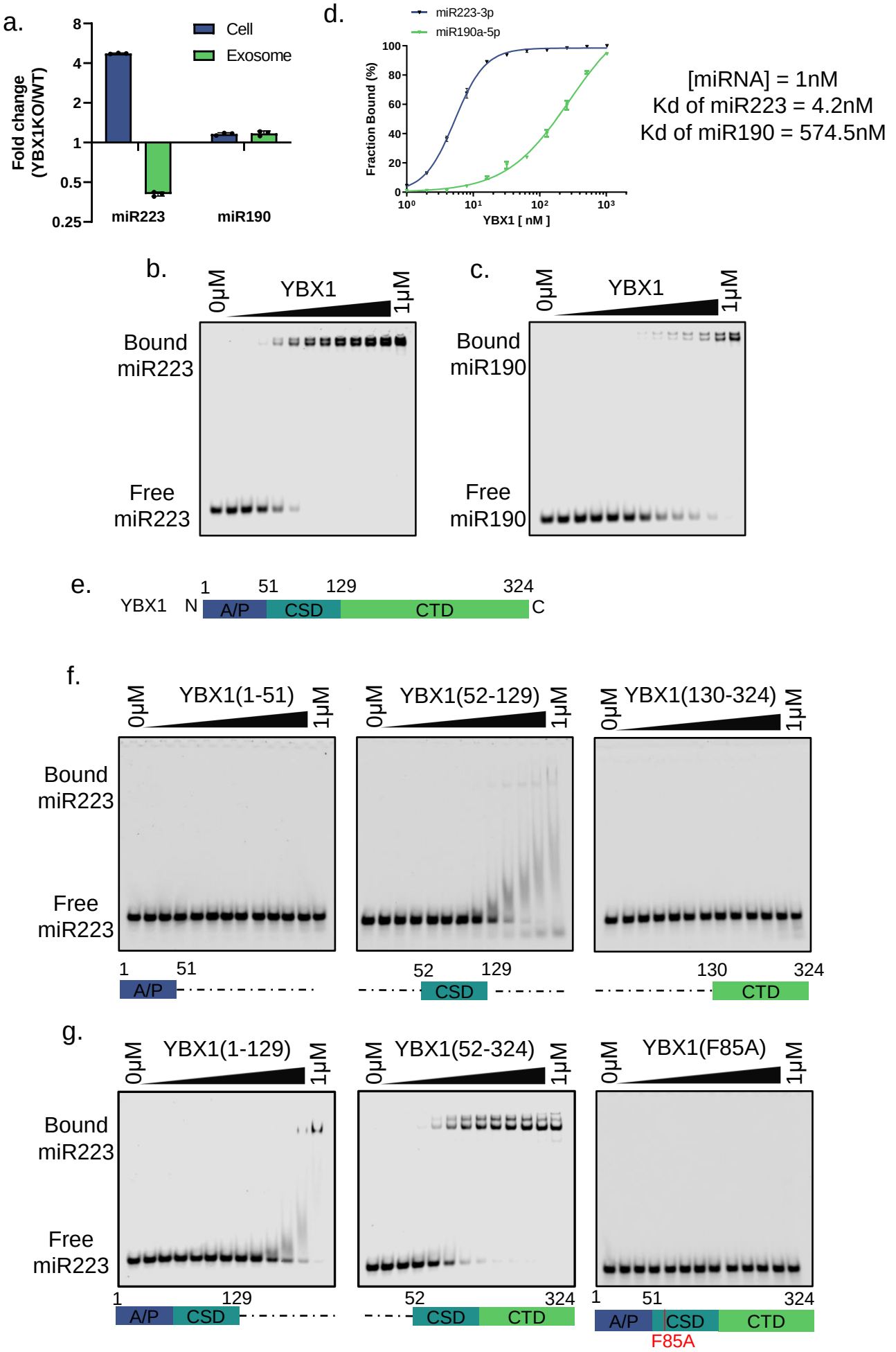

Figure 1-figure supplement 1. Knockout of YBX1 did not change exosome secretion.

a.

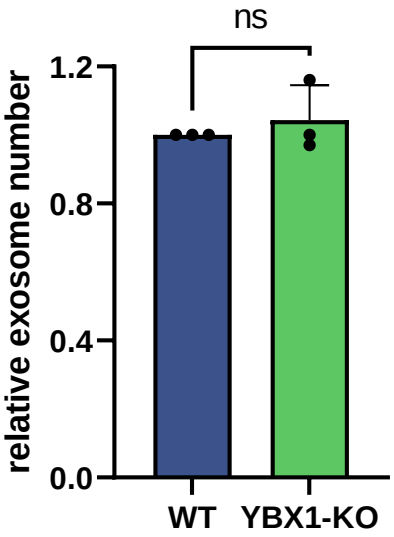

Figure 1-figure supplement 2. Purified YBX1 full length protein and different truncations and mutation

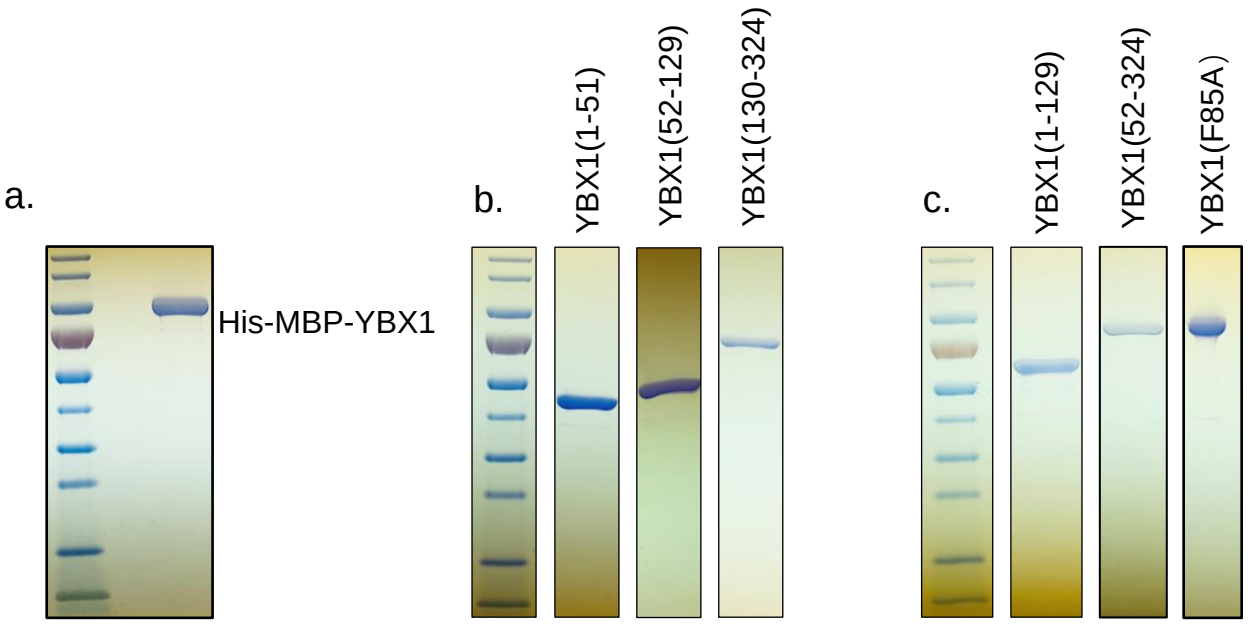

Figure 2. miR223 sequence motif UCAGU binds YBX1

a.

miR223-3p UGUCAGUUUGUCAAAUACCCCA
miR223mut UGAGACAUUGUCAAAUACCCCA

miR190-5p UGAUAUGUUUGAUAUAUUAGGU
miR190sort UGUCAGUUUGAUAUAUUAGGU

c.

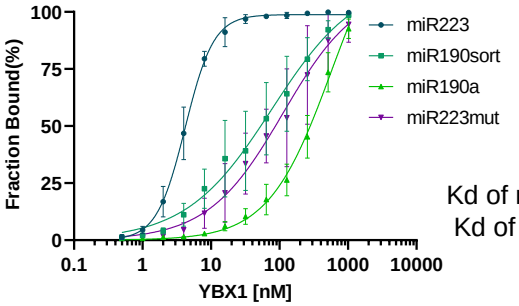

[miRNA] = 1nM
Kd of miR223mut = 112.4nM
Kd of miR190sort = 77.5nM

b.

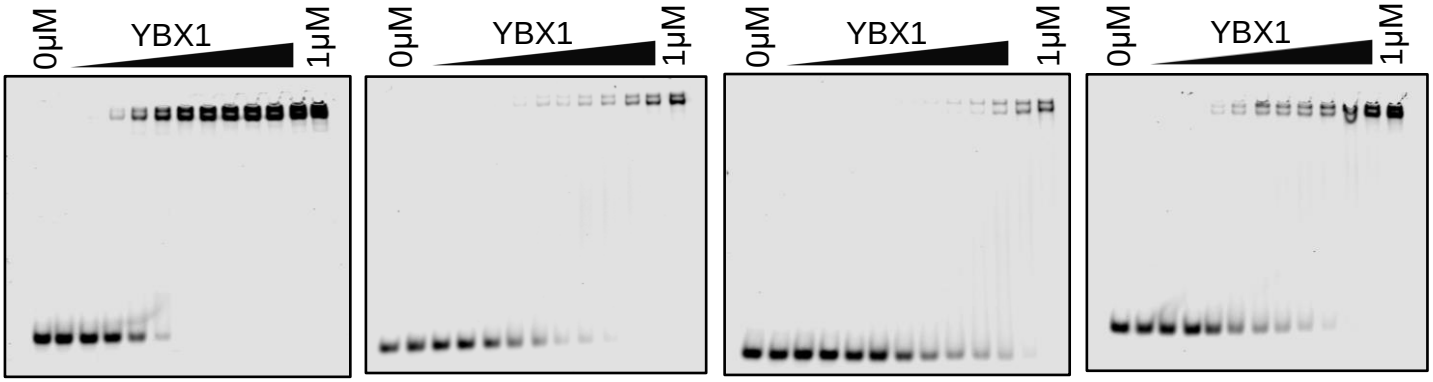

miR223 miR223mut miR190 miR190sort

d.

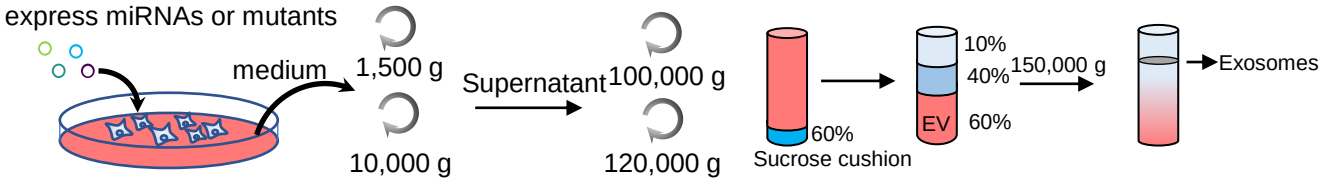

e.

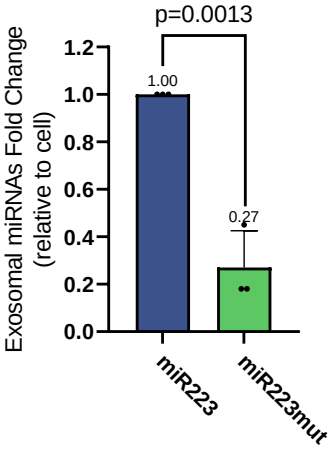

g.

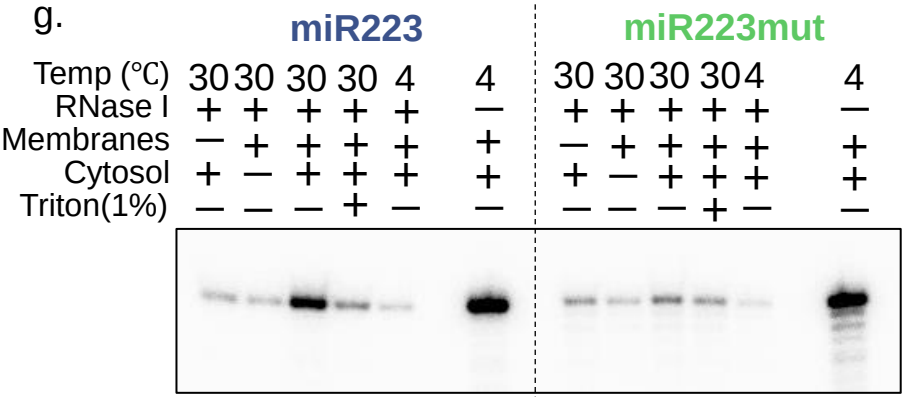

f.

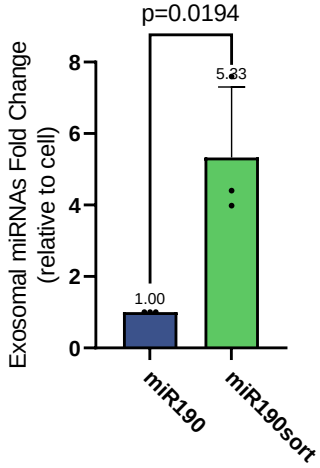

h.

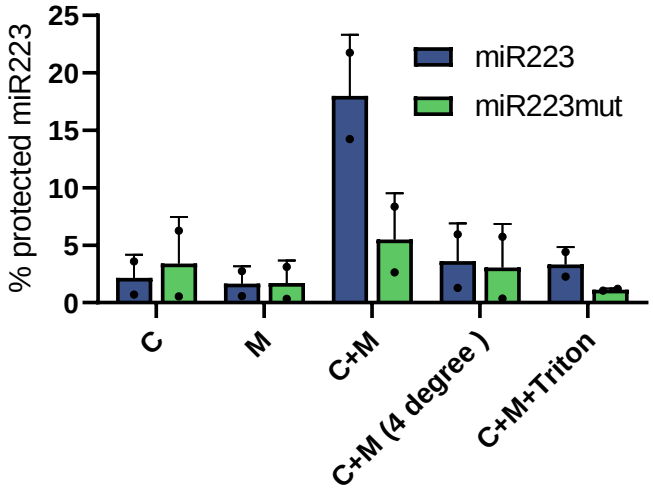

Figure 2-figure supplement 1. Screening exosomal sorting motif of miR223

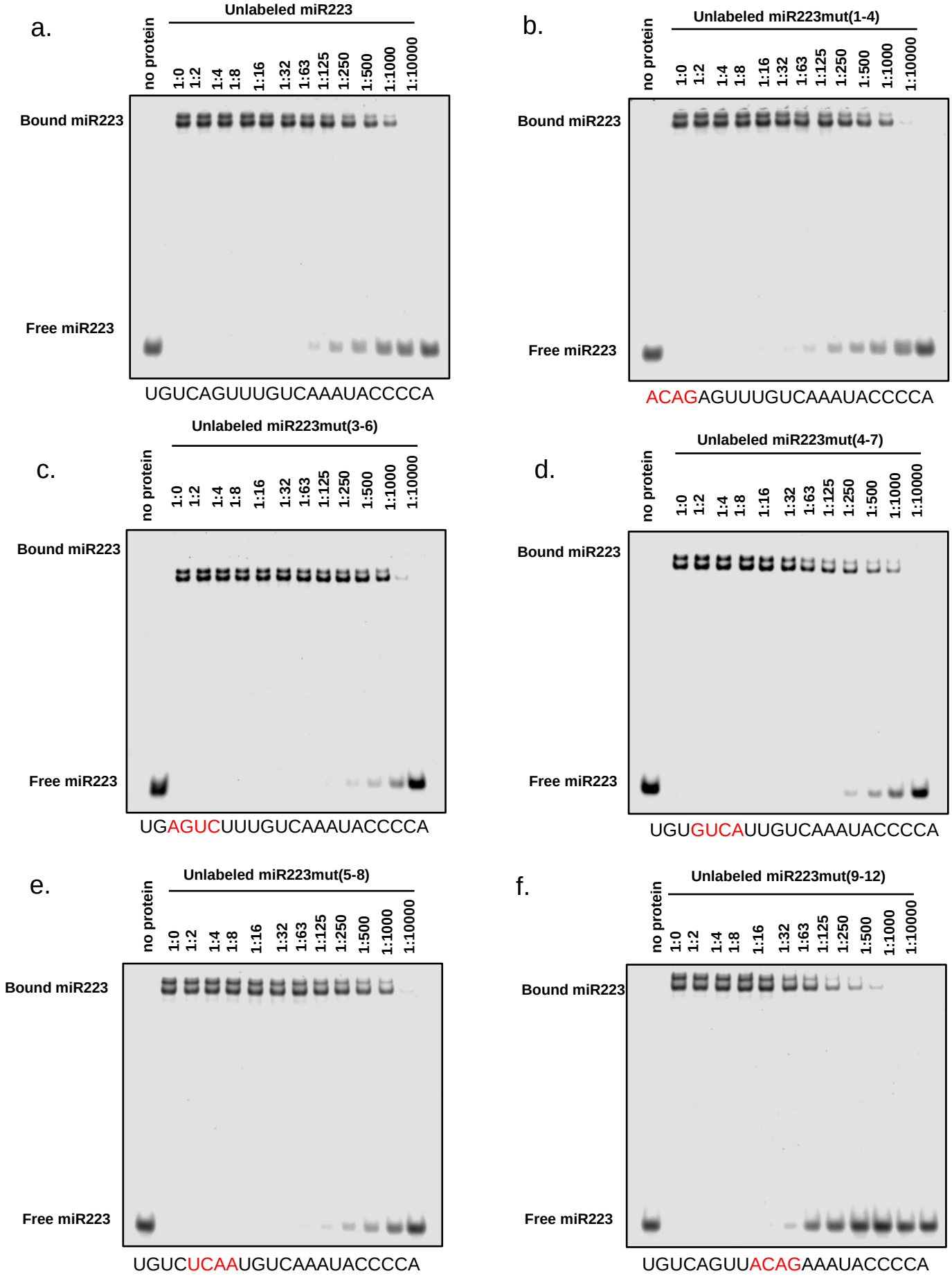

Figure 3. Mitochondria contribute to miR223 enrichment into exosomes

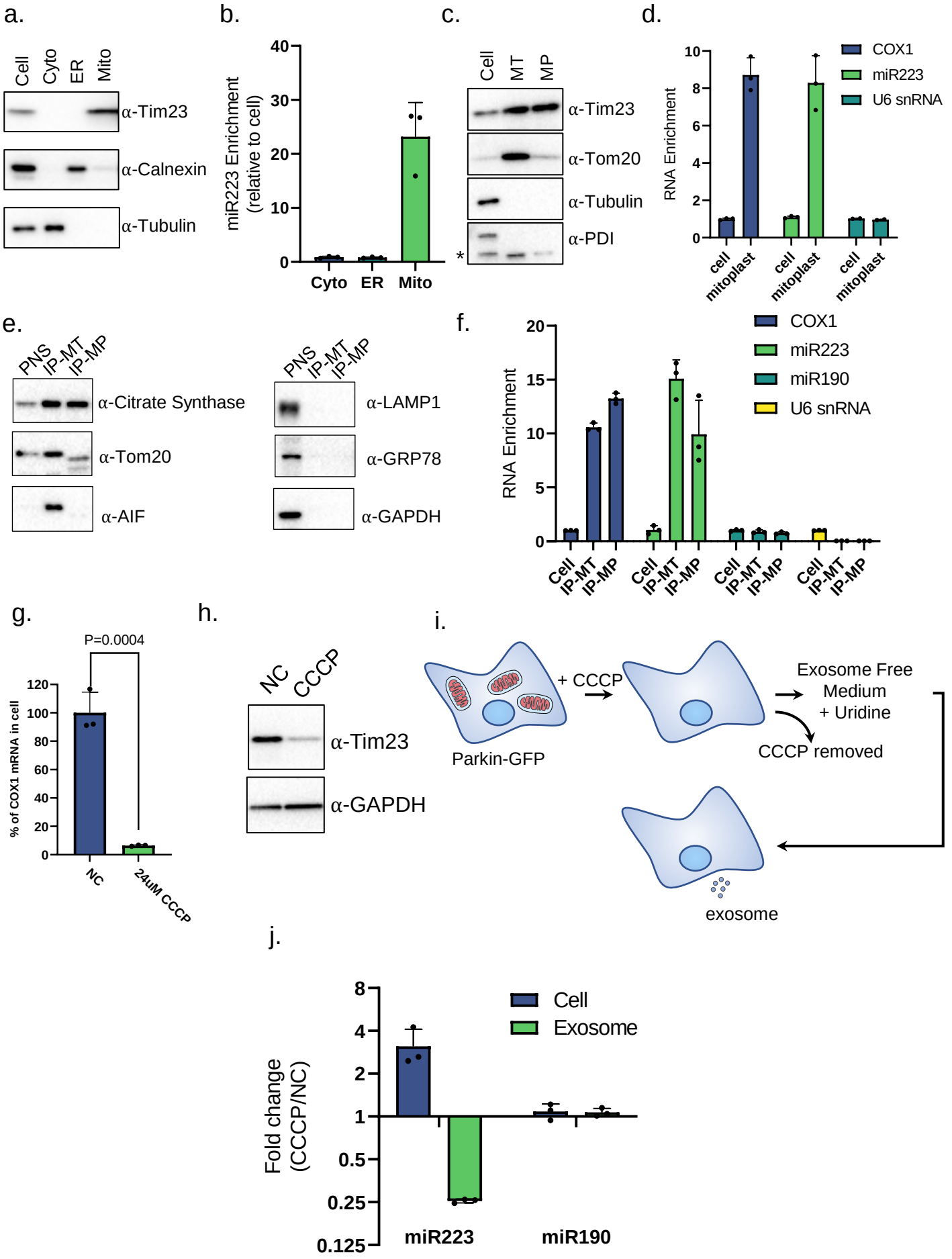

Figure 3-figure supplement 1. miR223, but not miR190, enriched in mitochondria.

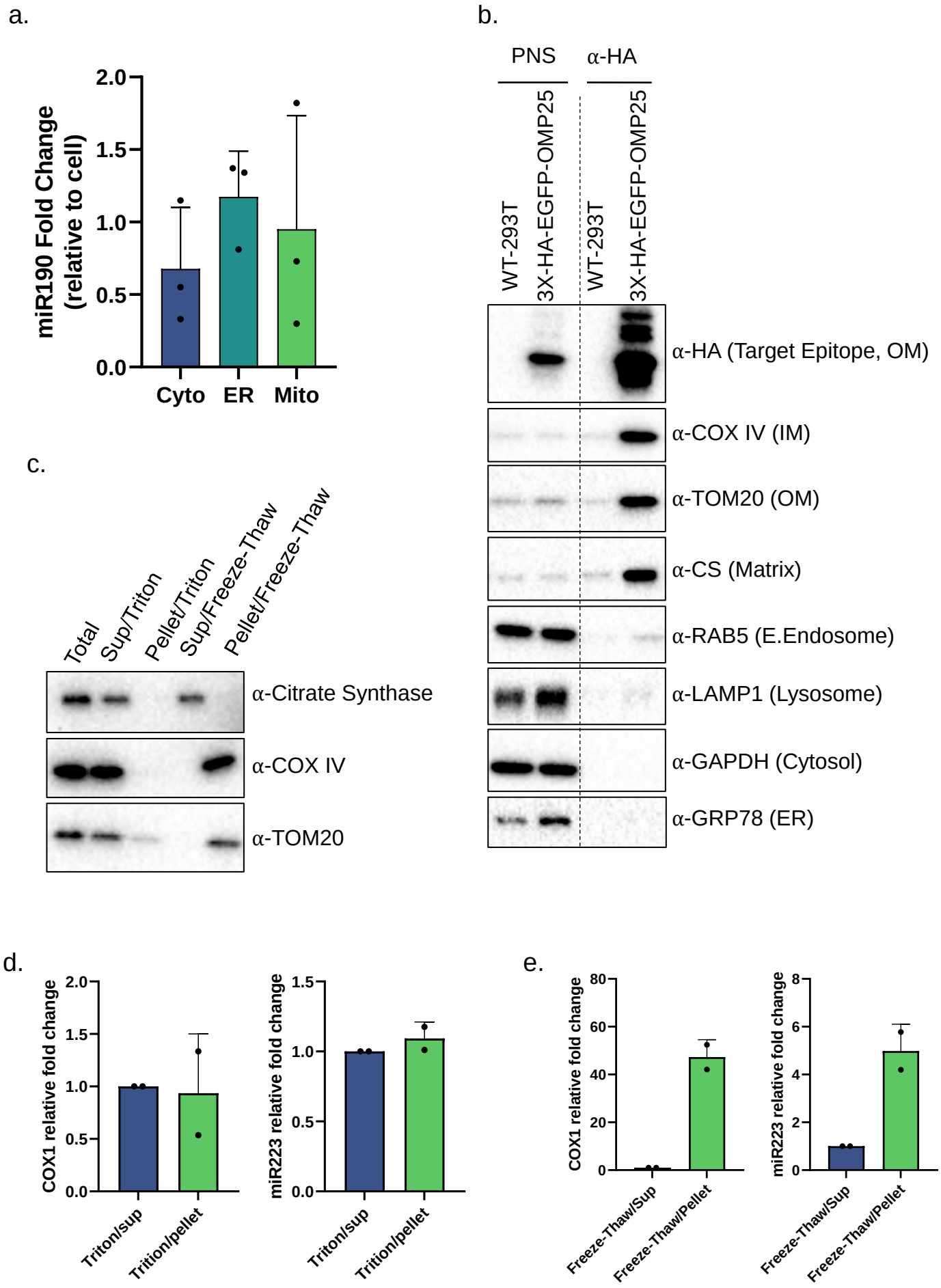

Figure 3-figure supplement 2. Mitochondrial depletion did not change exosome secretion.

a.

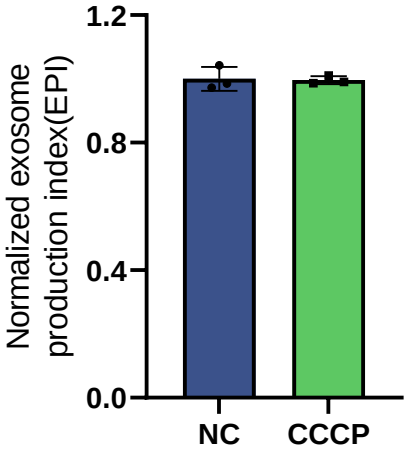

Figure 4. YBAP1 binds miR223 in the mitochondria and in vitro

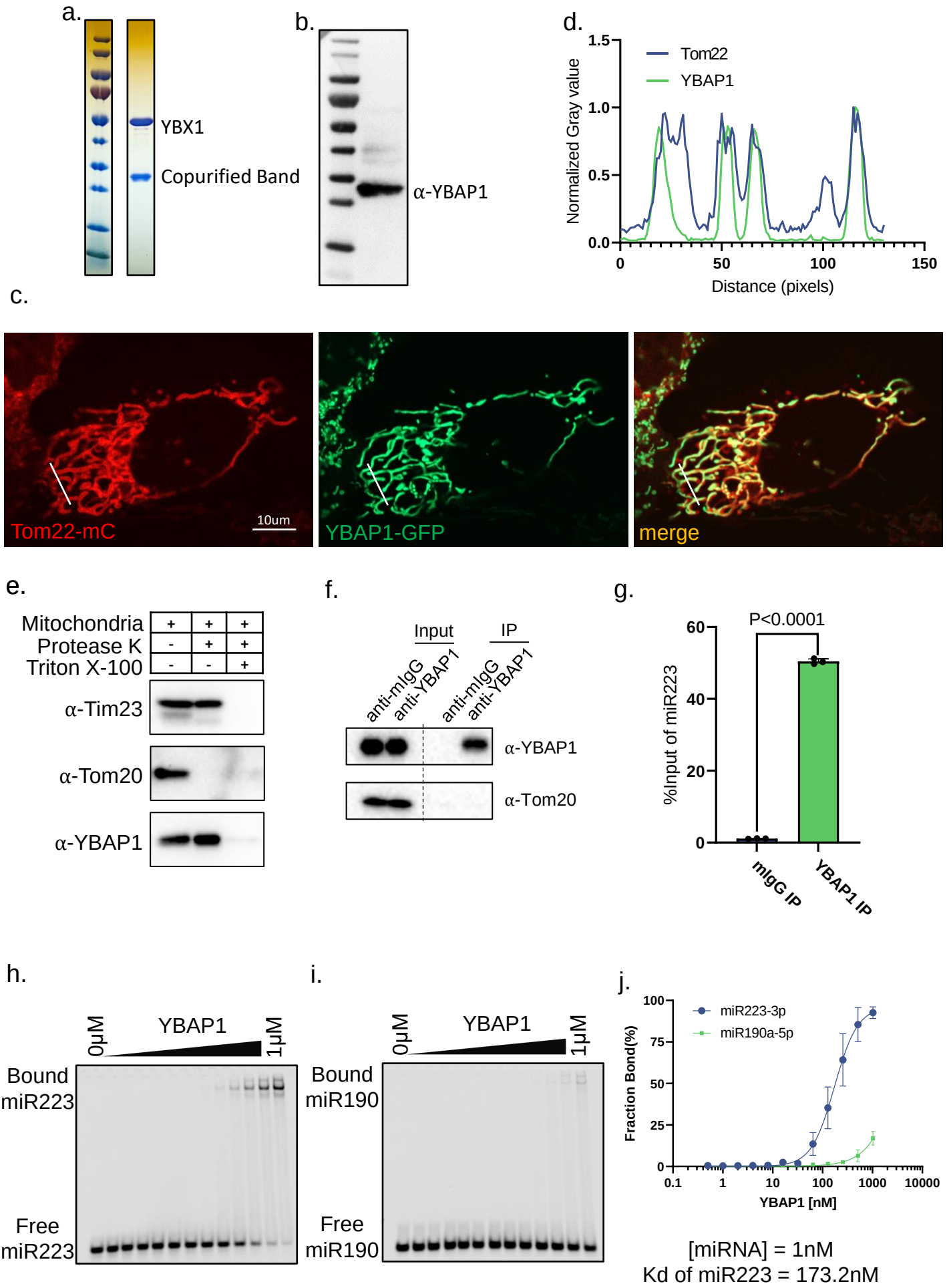

Figure 4-figure supplement 1. YBX1 and YBAP1 copurify as a complex from transfected SF9 cells.

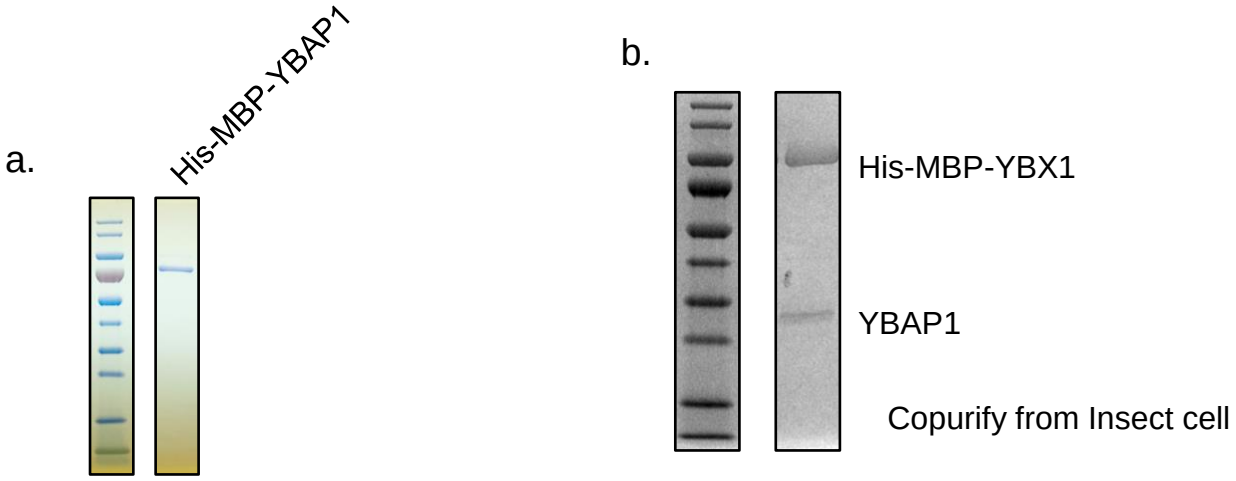

Figure 4-figure supplement 2. YBAP1 does not share the same motif as YBX1 that binds to miR223

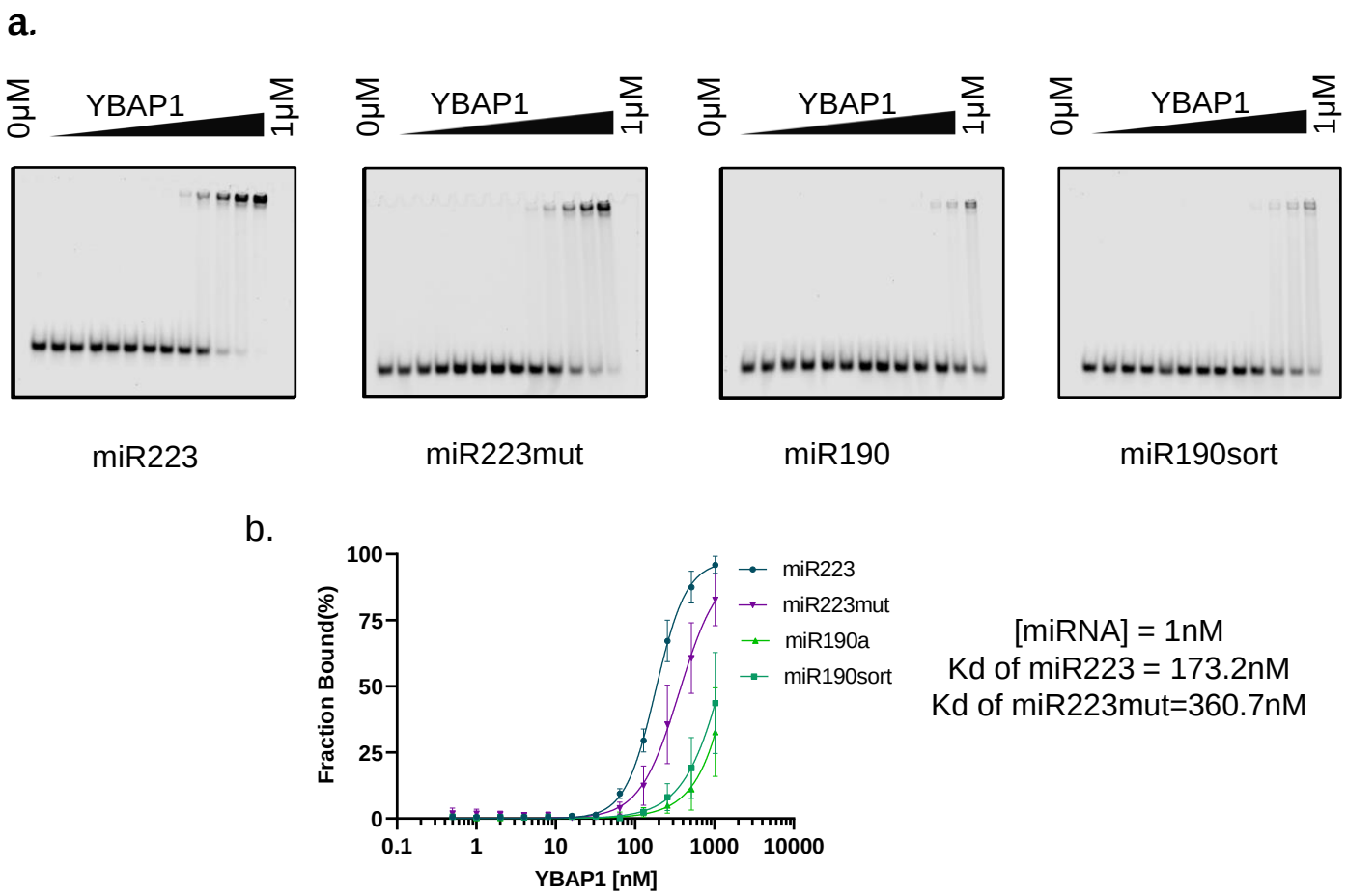

Figure 5 . YBAP1 sequesters miR223 which is released and secreted in YBAP1 KO cells

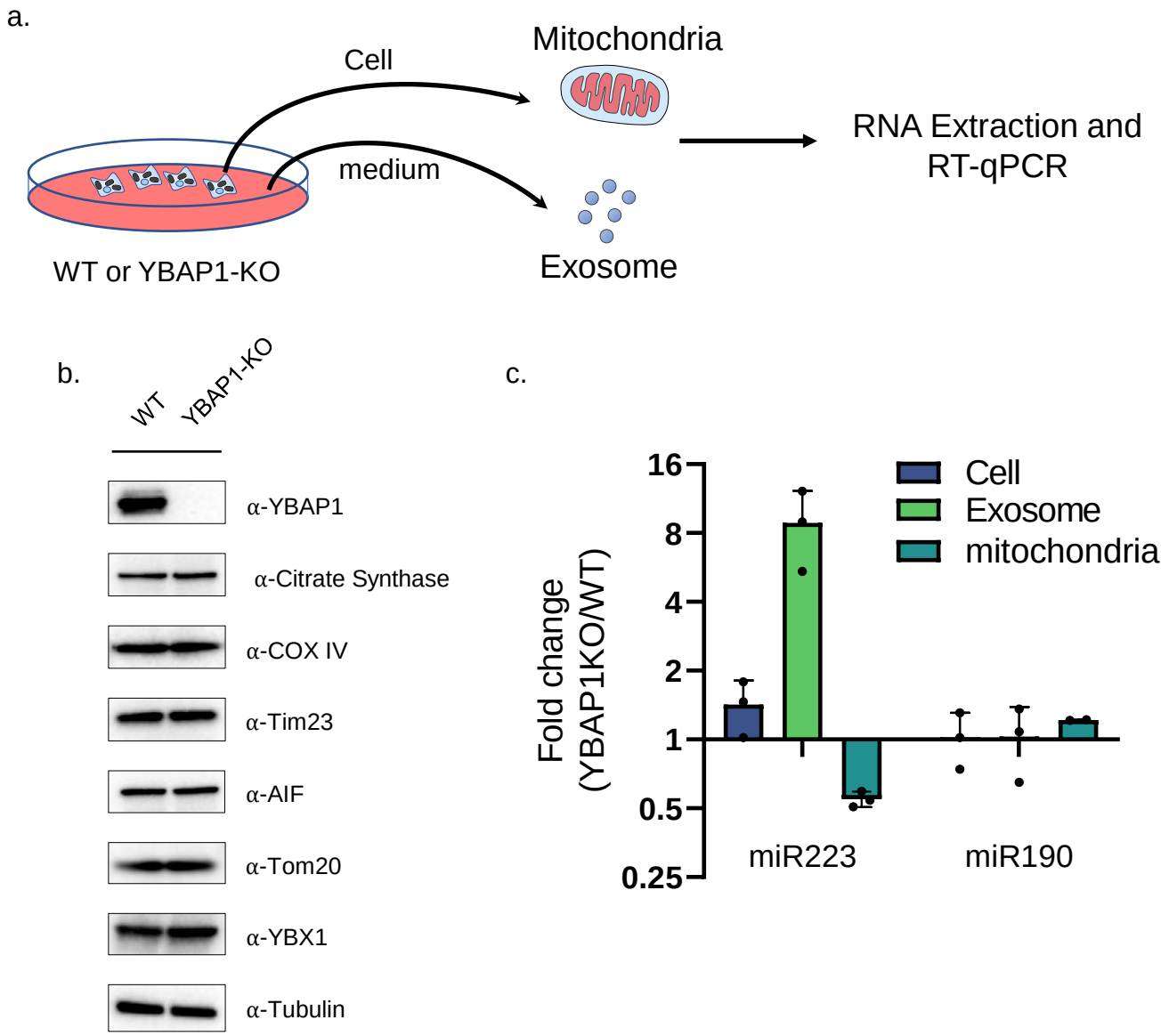

Figure 5-figure supplement 1. Knockout of YBAP1 did not change exosome secretion.

a.

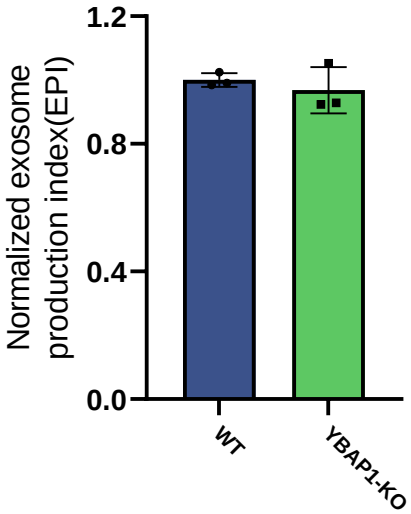

Figure 6. YBX1 puncta relocalize from mitochondria to endosomes

a.

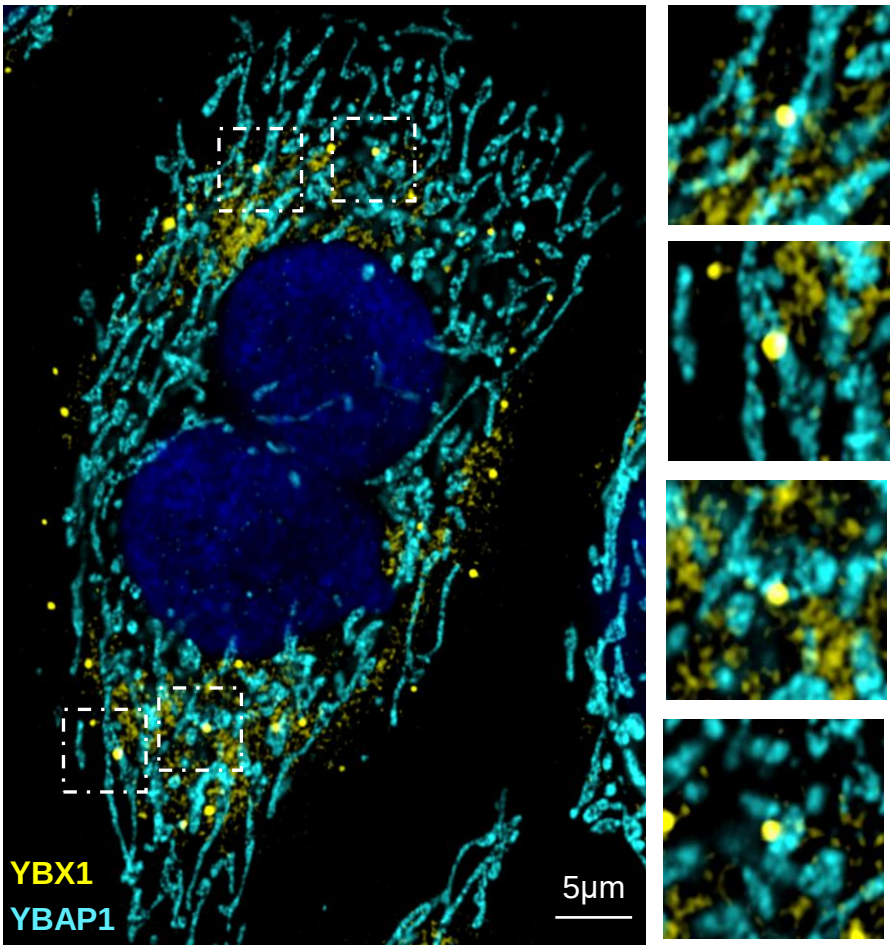

b.

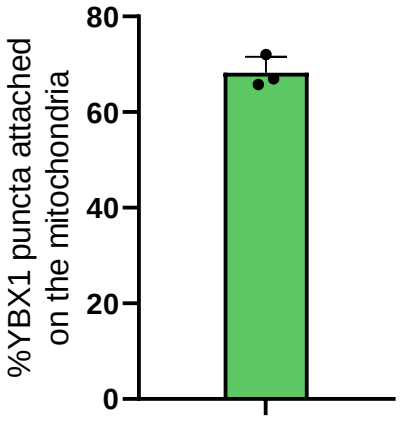

c.

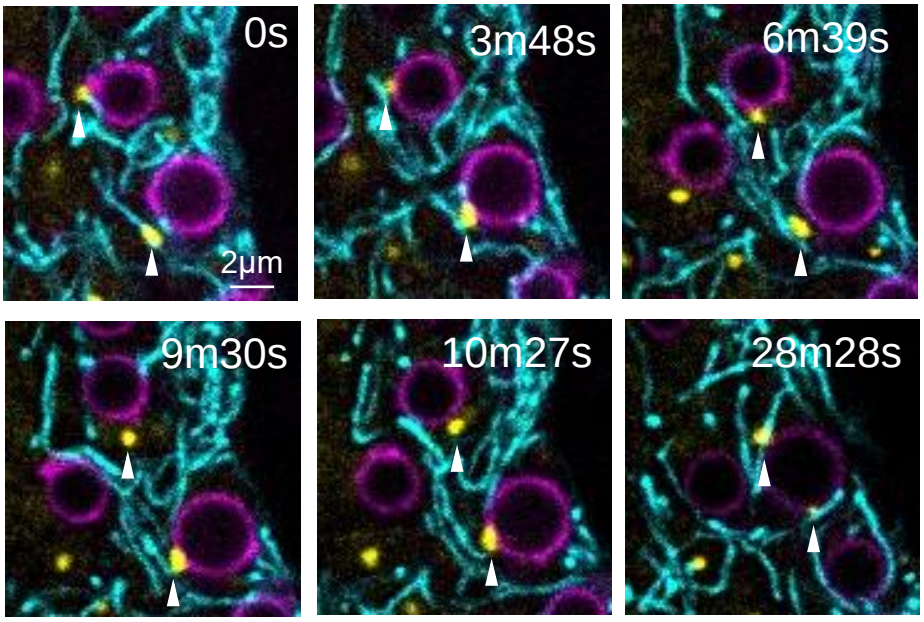

d.

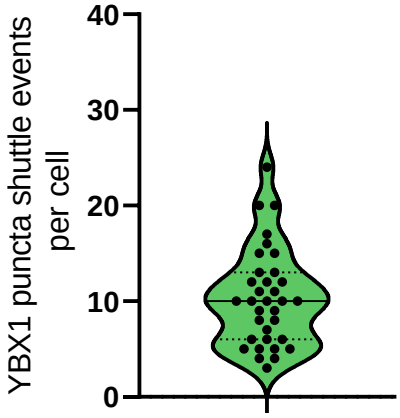
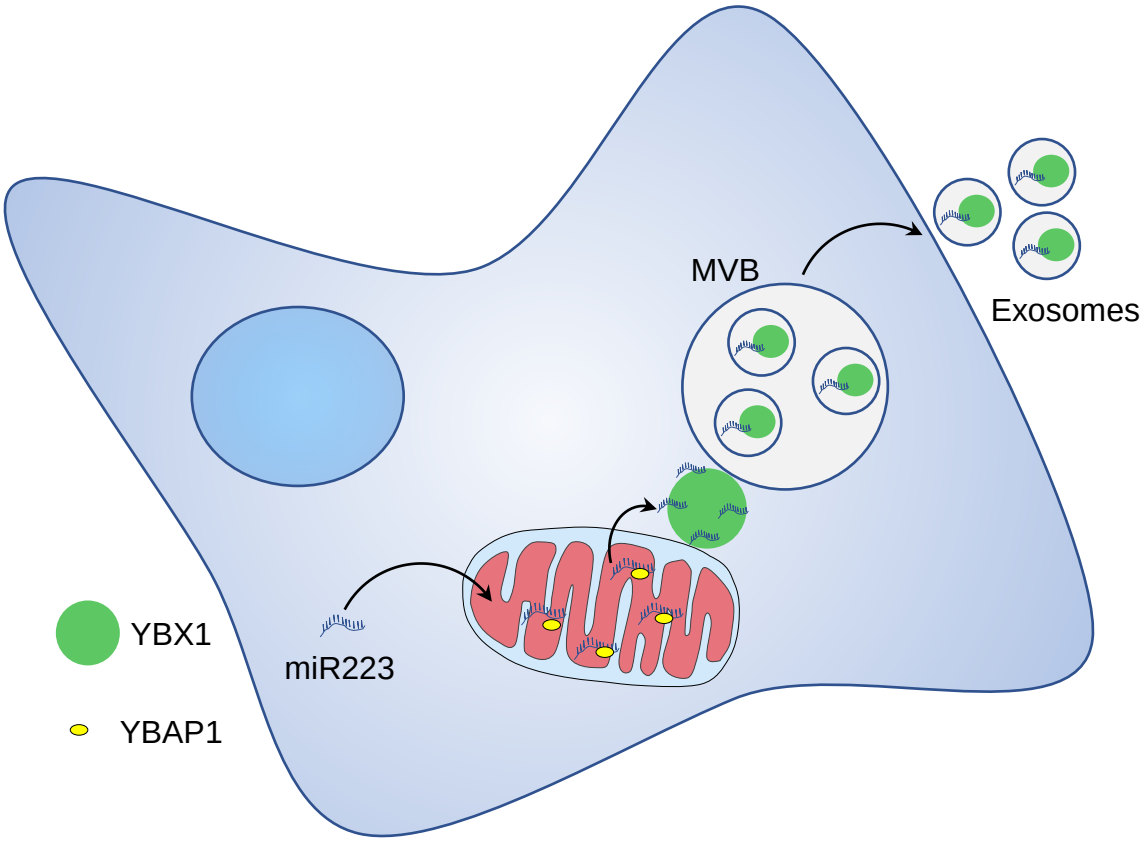
Figure 7. Diagram representing a model of miR223 sorting from mitochondria into exosomes